

We thank the reviewers for their valuable comments. Below we restate the comments in normal font and give our reply in *italics*. We hope that we have clarified everything and satisfactorily answered all the queries.

Reviewer #1

This paper emphasizes the need to think about how cover on a bedrock channel evolves, and I am supportive of that pursuit. I generally like the probabilistic approach of the paper. My review is not as deep as I would like it to be, because I got a bit lost in some of the details of the paper. I also had problems seeing how some of the sections tied together. Because the paper is so heavy in equations, and more importantly symbols, I think more reminders about what different symbols mean could make this a bit easier for the reader to follow. The table of symbols certainly helped. But anything the authors can do to improve the flow would be appreciated.

*We agree that we have many equations, but we do not think their number can be reduced without losing necessary mathematical detail (which would make the paper even more difficult to read to those who are only mildly enthusiastic about math...). In revisions, we have tried to clarify where possible.*

Line by line comments:

17 alleviated = alluviated?

*Corrected.*

Equation 3 : When I first read this, I thought “isn’t this probability actually a function of many things? Is there a reason that they only show it as  $A^*$  and  $M_s^*$ ?” It’s clear in the text that many variables are important, but I wondered why they were left out of the equation. Eventually I understood that the reason is because this paper focuses on  $A^*$  and  $M_s^*$ . Maybe this can be made clear from the start.

*We are not sure how to take this comment. We meant to indicate the possible dependence on other variables with the three little dots within the equation. The next sentence in the text makes explicit what we meant by this and gives a list of possible control parameters. We are not sure how to improve clarity here. Maybe the reviewer or the editor have a specific idea? [Text edited to try and clarify further.]*

Section 2.1 in general – I know that the authors are not going to change this, but I had a very hard time remembering that  $A^*$  is the fraction of exposed area, as in my head a cover function goes with fraction of area covered, not exposed. It’s not that the authors aren’t clear about the meaning, but somehow repeating the definition of  $A^*$  more would have helped me. For example, I suggest that on all figure axes words accompany symbols, so the meaning of the variable is not mistaken (as I did many times.) I also had a hard time getting used to the meaning of  $P$ . In retrospect, after reading line 124 it is clear. However I wonder if this could be emphasized somehow. E.g. State what  $P$  is on fig 1A y-axis, or at least restate in the caption. I know repetition is frowned upon in scientific writing, but I need it in this paper.

*We try to improve readability in the revisions by repeating the definitions of variables. In particular, we will revise the figures to give both a verbal description of the parameters and their symbol.*

*Nevertheless, we want to stress here that the exposed fraction, as we have used it, and not the covered fraction is the parameter that is commonly used in equations, because erosion rate is proportional to the exposed fraction.*

L 159: I've never seen the word run used like this. Exist instead maybe?  
*Changed as suggested.*

Section 2.2: Again I'm not quite sure that you can do anything about this, but I got confused here because now you are talking about the probability of entrainment, in contrast to above which was the probability of deposition. Maybe just make sure this is clear to readers.

*We have added qualifiers to make the relations more clear. To further avoid confusion, we have also changed to small font and added the symbols  $p_i$  and  $p_c$  to the notation list. We also added a sentence to the introductory paragraph, explaining the relation between  $p_c$  and  $p_i$  and the  $P$ -function.*

In this model all grains move the same length, right? So where they are deposited is not at all affected by whether or not there are grains in that location, right? This is confusing to me given that in the previous section deposition is probabilistic based on whether there are other grains present. So I had a hard time comparing this model with your framework.

*In the model sediment cover is only calculated for grains that are stationary for a time step; grains that are deposited and then immediately re-entrained do not count. Consequently the model implicitly incorporates the effect of local sediment cover on grain deposition. Note also that our  $P$ -function quantifies deposition on a reach-scale, while the formulation in the CA model is concerned with the grain scale. When grain scale dynamics are varied, this has a direct effect on the reach-scale, which is expressed in a different  $P$ -function. We have added some clarifying sentences.*

Figure 3: Is this plotting the probability of deposition or entrainment? I think I know the answer, but maybe make this clear.

*This is, of course, the probability  $P$  defined in eq. (3). We have tried to clarify.*

Equation 13 was hard for me. It seems like a new way to write this, but maybe you can walk me through it. Wouldn't  $E$  and  $D$  be included in  $d q_s / dx$ ? That is, wouldn't material be deposited if  $q_s$  decreased downstream and entrained if  $q_s$  increased downstream. I couldn't much evaluate this model because I didn't understand equation 13.

*We have explained the meaning of this equation in our brief reply in the discussion of the paper, which is reproduced below. We are at a little loss as how to deal with this comment. On the one hand, we can see that the reviewer was confused by this particular equation and as a result had a hard time understanding the remainder of the paper. On the other, the equation is a standard mass balance (derived from mass conservation), which is routinely used in river dynamics (in a slightly different form as Exner equation), geochemistry and many other disciplines. We think we have made these connections sufficiently clear in the introductory sentences preceding the presentation of the equation. Since a presentation of the derivation, including a cartoon, would take about half a page, we decided to not change the manuscript here. Nevertheless, we are willing to do so if the editor sees the necessity. Some of the confusion may arise because here we have two different reservoirs ( $M_m$  and  $M_s$ ) and so we need to explicitly represent the transitions between them, whereas in a classic Exner the transition of sediment between bedload and bed is assumed and not explicitly represented. That is, if there is a downstream decrease in bedload, in the Exner equation the excess sediment is assumed to be deposited, while we make the exchange between mobile and stationary particle reservoirs explicit. Apart from the obvious advantage when one is interested in the size of the stationary reservoir, which is related to bed cover, the role of particle speed becomes also explicit. We have added a sentence to clarify this relation..*

From our previous discussion: Here, we want to briefly comment on eq. 13 that the reviewer found hard to understand. This is a mass balance that is probably more easily understood when viewed in a discrete framework. Consider a mass balance for a control volume in the river (Fig. 1). The rate of change of mobile mass per time,  $\Delta Mm/\Delta t$  is then the sum of four terms: the mass influx per time from upstream  $\Delta in$ , the mass outflux per time downstream  $\Delta out$ , the entrained mass per time  $E$  and the deposited mass per time  $D$ . Both outflux  $\Delta out$  and deposition  $D$  reduce mass in the control volume and are therefore negative. Thus:

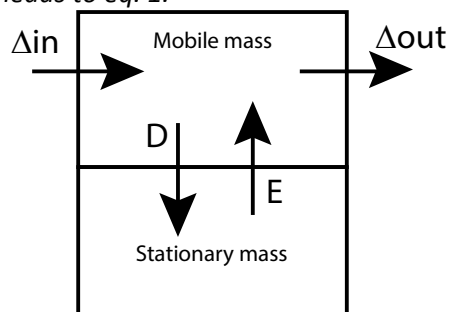
$$\Delta Mm/\Delta t = \Delta in - \Delta out + E - D$$

(eq. 1)

Our equation 13 is essentially a version of this equation where the long-stream variable and the time are treated as continuous corresponding to the limit of infinitesimal length of the control volume and infinitesimal time steps. In this limit the term  $\Delta in - \Delta out$  becomes  $dq_s/dx$  and the term  $\Delta Mm/\Delta t$  becomes  $dM/dt$ .

Note that this is essentially equivalent to the standard Exner equation, which is written in terms of bed height rather than mass, and thus wraps both our reservoirs (mobile and stationary) into a single equation. Since we are explicitly interested in the mass on the bed, and since bed height necessarily varies across a partially covered bed, we opted for using mass as a main variable.

Fig. 1: Cartoon illustration of a control volume in the river. The mass balance for the mobile mass  $Mm$  leads to eq. 1.



L 347: I think that this is  $E^*(M^*s = 0) = 0$ , right? If so, maybe state explicitly.  
*Changed as requested.*

L 417 – 419: I was confused about the comparison because you are not plotting the same thing as earlier plots. That is  $Q^*$  is not  $M_s^*$ , as was on the x-axes earlier. Can you help the reader relate these two variables?

This is correct. A main point of this chapter is to establish the relation between mass reservoirs  $Mm$  and  $Ms$  and the relative sediment supply  $Qs^*$ . This partly has historical reasons – the cover function has so far been expressed in terms of  $Qs^*$  (see, for example, Sklar and Dietrich, 2004), while experiments give the relation to  $Ms$  (see, for example, Sklar and Dietrich, 2001). The transformation between these two variables has been often overseen or done wrong (including in one of the first author's earlier papers, Turowski et al., 2007). So, one of the aims of this chapter is the clarification of this particular relationship and the provision of a sound physical basis to model it. We have added a few sentences at the beginning of the chapter to clarify this aim.

$Q^*$  is also not defined in your notation.

Is  $Q^*$  on the x-axes in figure 4 supposed to be  $Q^*_s$  with a bar over it? Maybe same for Figure 5 and also in the caption of figure 4?

*Sorry, this was carried over from an early version of the manuscript. Of course we meant  $Q^*_s$ . We have corrected throughout.*

L 465 Where did 5.7/11.5 come from?

*These are dimensionless constants determined from experiment by Fernandez-Luque and van Beek (1976). See equations 35/36. We provided a reference to these equations and the text has been edited for clarification.*

Figure 10A – the x-axis is not formatted correctly.

*We do not see exactly the problem the reviewer tries to point out. However, we have revised all figures to improve clarity and readability.*

Sentence starting on L 611: Does this mean that  $A^* = 0$  at all times?

*In the natural channel bed of the Erlenbach, yes. But this is irrelevant here, as we were trying to say with the criticized sentence. We merely use the measured time series of bedload transport and discharge to supply realistic input data. We have revised the introduction to the chapter to make this clear.*

I guess this gets to a point that I didn't understand in the previous section - when you are talking about the evolution of the mass on the bed through time, this could be under conditions of complete cover the entire time. It might be worth stating this directly. Although I'm not sure that I'm correct about this assumption. In Figure 12, assuming that A on the second from top plot is actually  $A^*$ , implies that there is not complete cover. I don't think I understood this section very well.

*Yes, of course, the cover can be complete all the time. In the simulations we present here for the Erlenbach, the final cover state depends strongly on the initial cover state. This indicates that during the event, there was not enough time to reach a steady cover state. If we had started the simulation with full cover, it would have stayed full for the entire event.*

*That said, the temporal evolution is also strongly dependent on how one calculates transport capacity, which is a thorny issue for steep streams such as the Erlenbach. We have normalized our transport capacity such that the ratio of supply to capacity is equal to one at the highest discharge. Thus, during most of the event, relative sediment supply is smaller than one (in effect, by choice). The point here was to show the cover evolution for realistic boundary conditions as an illustrative example, rather than trying to predict bed cover throughout an event for the Erlenbach. We have rephrased to improve clarity.*

Also in this section, in a single flood event I'm having a hard time understanding what the meaning of  $p$ , or the period is. The previous section discussed the period in terms of a sine wave in sediment supply. But is that the case for this flood?

*This is meant to be the same as the period discussed earlier. In essence, we assumed that at each time step, a new sinusoidal perturbation with a fixed amplitude commences. From the data we can estimate the local gradient in the variables and use this to calculate an 'effective' period. We agree that we had not done a good job in explaining this and have tried to improve.*

Sentence starting on L 669: This is great. Is this shown explicitly and I didn't catch it?

If not, can you spell this out more directly?

*As is explained in the paragraphs preceding this statement, it is currently not that easy to provide direct comparisons with data or calibrate the P-function directly, mainly because the necessary parameters have not been reported in the experimental studies. However, we have directly demonstrated that the formulation is flexible enough to yield a wide range of cover*

functions (see Figs. 4 and 5 for examples). These do encompass (most of) the relationships observed in laboratory and numerical experiments. We do not think that we can meaningfully go any further at the moment, but have provided a reference to the figures.

L 678: This dynamics cover ... typo I think.  
*Typo; corrected.*

Sentence starting on Line 735 has a typo.  
*Indeed; corrected.*

Section 4.3: The comparison with Philips and Jerolmack is a bit confusing to me. You state that in contrast to their findings, your findings suggest that bed cover is adjusted. But you didn't actually have channel morphology as a free variable. So I'm not sure how this study can contrast that one. I don't remember exactly, but I don't think they talked about sediment cover. So is this a fair way to compare the two studies?

I like how your conclusions stated this issue - both cover and channel morphology evolve. This makes sense to me, but the discussion in section 4.3 did not.

*Here, a main point is that bedrock rivers can adjust cover to achieve grade. And this can be done much more rapidly than adjusting channel morphology. Philips and Jerolmack missed this mechanism – they argue that in bedrock channels, morphological adjustment needs to be quick, because they observe graded channels. But, as stated, the river has other options to achieve grade – by adjusting bed cover. We have rewritten the entire paragraph to clarify.*

Reviewer #2

In this manuscript, the authors presented a probabilistic framework for predicting partial cover in mixed bedrock-alluvial channels, which they used to explore how probability of sediment deposition, relative sediment supply, and particle speed interact. It represents a next step in the progress that has been made over the past several years in modeling areal fraction of sediment cover. Overall, I found this to be a good paper, with sound methods and interesting results.

*We thank the reviewer for this assessment and the comments. We hope that in our revisions we can satisfactorily answer all queries.*

1. My main concern with the manuscript is the equations for entrainment rate and deposition rate. Although the authors explain that eq. 20 approaches  $E_{max}^*$  as  $M_s^*$  goes to infinity, does the same apply to eq. 21? I think  $M_m^*$  cannot be infinity because it is limited by the capacity value  $M_0^*$ . If so, when  $M_s^*$  is very large, it is impossible to balance  $D$  with  $E$ .

*$M_m$  is related to particle speed and upstream sediment supply via equation (24). Since both of these other variables are treated as input parameters,  $M_m$  is fixed by them (at steady state).  $M_m$  can only become infinite in the non-physical cases of zero particle speed but finite transport rate, or infinite supply. The deposition rate is then set by eq. (21). If  $M_m$  is large (i.e., enough sediment is available), deposition is limited by upstream sediment supply. In essence, eq. (21) states that when  $M_m$  is small, the amount that can be deposited is limited by  $M_m$  (if there is only one mobile particle available, then a maximum of one can be deposited), and if  $M_m$  is large, deposition is limited by sediment supply. This explanation has been added to the text.*

2. The authors assume that increasing sediment deposition decreases local shear stress and increases the critical entrainment shear stress for grains (Line 186-192 and 242-245). I think this assumption is limited to the case of smooth bedrock. Sediment deposition does not necessarily decrease the flow velocity. In rough bedrock, increasing sediment deposition increases local shear stress and decreases the critical shear stress for grains.

*This is a good point that we have taken up in the discussion. Indeed, we were thinking of smooth rather than rough bedrock. We have added 'smooth' at the appropriate places to qualify. In addition, feedbacks between cover and roughness have been discussed in some depth in the introduction.*

3. In section 4.2, although the authors explain the differences from the model presented by Nelson and Seminara (2011, 2012); the model presented in this paper has more similarities to the model presented by Inoue et al. (2014). In the mentioned paper, they have distinguished between mobile and stationary sediment, and have not assumed a direct correspondence between sediment concentration and degree of cover, which is different from Nelson and Seminara (2011, 2012). I think the main difference is in the sediment continuity equation including entrainment rate and deposition rate. This equation seems very useful. I encourage the authors to explain the differences from Inoue et al. (2014) and the advantages of this sediment continuity equation.

*We have included an additional paragraph discussing this model.*

Additional comments by line number below:

Line 140: There are situations when sediment does not accumulate even if the exposed part is zero. For example, runaway alluviation in Chatanantavet and Paker (2008).

*We are aware of this mechanism and mention it several times in the manuscript. In principle, the mechanism can be modelled in the framework, but entrainment and deposition rate for this case need to be dependent on the state of cover. As a purely descriptive tool, the P-function will still work (there is an example of run-away alluviation in the model data). There could potentially also be hysteresis in cover, which could be modelled by separate P-functions for entrainment and deposition. This is, however, beyond the scope of the paper, in particular as there are currently no data available to constrain the P-function for laboratory experiments or natural channels. We do not see why the reviewer made this statement in relation to line 140 of the manuscript. All statements there are general and correct.*

Line 242-245: It is good to describe a physical reason for smoothing.

Smoothing is applied to prevent the formation of unrealistic piles of grains in one cell when there are far fewer grains in adjacent cells. The text was edited to explain.

Line 345: Can  $(1 - e^{-Ms})qt^*$  be converted to  $(1 - A)qt^*$ ? If so, the entrainment rate is proportional to the areal fraction of sediment cover.

*Only for the assumption  $P=A^*$ . We work with this assumption a lot in the later interpretation of the equations and in examples, but at this point, P is left general. But this is a nice way of looking at it.*

Figure 4 and Figure 5:  $Q^* = Q_s^*$ ?

*Apologies, this was a mistake.*

Figure 7: What is arbitrary unit? Is the sediment supply rate specified?

*One uses arbitrary units when the absolute scale of the relation is irrelevant for the argument.*

Figure 8: Please explain the distance from upstream end to downstream end, transport

capacity, bed slope and grain size.

*All the variables mentioned by the reviewer are not relevant – what is relevant is not the absolute transport capacity, but the relative sediment supply (supply normalized by transport capacity).*

*We have worked here in the non-dimensional framework specified in 3.1. We have revised the caption for Figure 8, including references to the relevant equation and the one variable that we had missed, particle speed. All relevant information is now contained in the caption.*

Figure10: Which equations are used to calculate 99% response time?

*We used numerical solutions to obtain these data. The corresponding equations in the paper are (3), (22), (23) and (24). The text has been added to clarify.*

# 1 A probabilistic framework for the cover effect in bedrock erosion

2  
3  
4 Jens M. Turowski

5 *Helmholtzzentrum Potsdam, German Research Centre for Geosciences GFZ, Telegrafenberg, 14473*  
6 *Potsdam, Germany, turowski@gfz-potsdam.de*

7 Rebecca Hodge

8 *Department of Geography, Durham University, Durham, DH1 3LE, United Kingdom,*  
9 *rebecca.hodge@durham.ac.uk*

## 10 11 12 Abstract

13 The cover effect in fluvial bedrock erosion is a major control on bedrock channel morphology and  
14 long-term channel dynamics. Here, we suggest a probabilistic framework for the description of the  
15 cover effect that can be applied to field, laboratory and modelling data and thus allows the  
16 comparison of results from different sources. The framework describes the formation of sediment  
17 cover as a function of the probability of sediment being deposited on already alluviated areas of the  
18 bed. We define benchmark cases and suggest physical interpretations of deviations from these  
19 benchmarks. Furthermore, we develop a reach-scale model for sediment transfer in a bedrock  
20 channel and use it to clarify the relations between the sediment mass residing on the bed, the  
21 exposed bedrock fraction and the transport stage. We derive system time scales and investigate  
22 cover response to cyclic perturbations. The model predicts that bedrock channels achieve grade in  
23 steady state by adjusting bed cover. Thus, bedrock channels have at least two characteristic time  
24 scales of response. Over short time scales, the degree of bed cover is adjusted such that they can just  
25 transport the supplied sediment load, while over long time scales, channel morphology evolves such  
26 that the bedrock incision rate matches the tectonic uplift or base level lowering rate.

## 27 28 1. Introduction

29  
30 Bedrock channels are shaped by erosion caused by countless impacts of the sediment particles they  
31 carry along their bed (Beer and Turowski, 2015; Cook et al., 2013; Sklar and Dietrich, 2004). There are  
32 feedbacks between the evolving channel morphology, the bedload transport, and the hydraulics  
33 (e.g., Finnegan et al., 2007; Johnson and Whipple, 2007; Wohl and Ikeda, 1997). Impacting bedload  
34 particles driven forward by the fluid forces erode and therefore shape the bedrock bed. In turn, the  
35 morphology of the channel determines the pathways of both sediment and water, and sets the stage  
36 for the entrainment and deposition of the sediment (Hodge and Hoey, 2016). Sediment particles play  
37 a key role in this erosion process; they provide the tools for erosion and also determine where  
38 bedrock is exposed such that it can be worn away by impacting particles (Gilbert, 1877; Sklar and  
39 Dietrich, 2004).

40  
41 The importance of the cover effect - that a stationary layer of gravel can shield the bedrock from  
42 bedload impacts – has by now been firmly established in a number of field and laboratory studies  
43 (e.g., Chatanantavet and Parker, 2008; Finnegan et al., 2007; Hobbey et al., 2011; Johnson and  
44 Whipple, 2007; Turowski and Rickenmann, 2009; Turowski et al., 2008; Yanites et al., 2011).

45 Sediment cover is generally modelled with generic relationships that predict the decrease of the  
46 fraction of exposed bedrock area  $A^*$  with the increase of the relative sediment supply  $Q_s^*$ , usually  
47 defined as the ratio of sediment supply to transport capacity. Based on laboratory experiments and  
48 simple modeling, Turowski and Bloem (2016) argued that the focus on covered area is generally



49 justified on the reach scale and that erosion of bedrock under a thin sediment cover can be  
50 neglected. However, the behavior of sediment cover under flood conditions is currently unknown  
51 and the assumption that the cover distribution at low flow is representative for that at high flow may  
52 not be justified (cf. Beer et al., 2016; Turowski et al., 2008).

53

54 The most commonly used function to describe the cover effect is the linear decline (Sklar and  
55 Dietrich, 1998), which is the simplest function connecting the steady state end members of an empty  
56 bed when relative sediment supply  $Q_s^* = 0$  and full cover when  $Q_s^* = 1$ :

57

$$A^* = \begin{cases} 1 - Q_s^* & \text{for } Q_s^* < 1 \\ 0 & \text{otherwise} \end{cases}$$

58 (eq. 1)

59 In contrast, the exponential cover function arises under the assumption that particle deposition is  
60 equally likely for each part of the bed, whether it is covered or not (Turowski et al., 2007).

61

$$A^* = \begin{cases} \exp(-Q_s^*) & \text{for } Q_s^* < 1 \\ 0 & \text{otherwise} \end{cases}$$

62 (eq. 2)

63 Here,  $\exp$  denotes the natural exponential function.

64

65 Hodge and Hoey (2012) obtained both the linear and the exponential functions using a cellular  
66 automaton (CA) model that modulated grain entrainment probabilities by the number of  
67 neighbouring grains. However, consistent with laboratory flume data, the same model also produced  
68 other behaviours under different parameterisations. One alternative behavior is runaway alluviation,  
69 which was attributed by Chatanantavet and Parker (2008) to the differing roughness of bedrock and  
70 alluvial patches. Due to a decrease in flow velocity, an increase in surface roughness and differing  
71 grain geometry, the likelihood of deposition is higher over bed sections covered by alluvium  
72 compared to smooth, bare bedrock sections (Hodge et al., 2011). This can lead to rapid alluviation of  
73 the entire bed once a minimum fraction has been covered. The relationship between sediment flux  
74 and cover is also affected by the bedrock morphology; flume experiments have demonstrated that  
75 on a non-planar bed the location of sediment cover is driven by bed topography and hydraulics (e.g.,  
76 Finnegan et al., 2007; Inoue et al., 2014). Johnson and Whipple (2007) found that stable patches of  
77 alluvium tended to form in topographic lows such as pot holes and at the bottom of slot canyons,  
78 whereas Hodge and Hoey (2016) found that local flow velocity also controls sediment cover location.

79

80 The relationship between roughness, bed cover and incision was explored in a number of recent  
81 numerical modeling studies. Nelson and Seminara (2011, 2012) were one of the first to model the  
82 impact that the differing roughness of bedrock and alluvial areas has on sediment patch stability.  
83 Zhang et al. (2014) formulated a macro-roughness cover model, in which sediment cover is related to  
84 the ratio of sediment thickness to bedrock macro-roughness. Aubert et al. (2016) directly simulated  
85 the dynamics of particles in a turbulent flow and obtained both linear and exponential cover  
86 functions. Johnson (2014) linked erosion and cover to bed roughness in a reach-scale model. Using a  
87 model formulation similar to that of Nelson and Seminara (2011), Inoue et al. (2016) reproduced bar  
88 formation and sediment dynamics in bedrock channels. All of these studies used slightly different  
89 approaches and mathematical formulations to describe alluvial cover, making a direct comparison  
90 difficult.

91

92 Over time scales including multiple floods, the variability in sediment supply is also important (e.g.,  
93 Turowski et al., 2013). Lague (2010) used a model formulation in which cover was written as a

94 function of the average sediment depth to upscale daily incision processes to long time scales. He  
 95 found that over the long term, cover dynamics are largely independent of the precise formulation at  
 96 the process scale and are rather controlled by the magnitude-frequency distribution of discharge and  
 97 sediment supply. Using the CA model of Hodge and Hoey (2012), Hodge (in press) found that, when  
 98 sediment supply was very variable, sediment cover was primarily determined by the recent history of  
 99 sediment supply, rather than the relationships identified under constant sediment fluxes.

100  
 101 So far, it has been somewhat difficult to compare and discuss the different cover functions obtained  
 102 from theoretical considerations, numerical models, and experiments, since a unifying framework and  
 103 clear benchmark cases have been missing. Here, we propose such a framework, and develop type  
 104 cases linked to physical considerations of the flow hydraulics and sediment erosion and deposition.  
 105 We show how this framework can be applied to data from a published model (Hodge and Hoey,  
 106 2012). Furthermore, we develop a reach-scale erosion-deposition model that allows the dynamic  
 107 modeling of cover and prediction of steady states. Thus, we clarify the relationship between cover,  
 108 deposited mass and relative sediment supply. As part of this model framework we investigate the  
 109 response time of a channel to a change in sediment input, which we illustrate using data from a  
 110 natural channel.

## 111 2. A probabilistic framework

### 112 2.1. Development

113  
 114 Here we build on the arguments put forward by Turowski et al. (2007) and Turowski (2009). Consider  
 115 a bedrock bed on which sediment particles are distributed. We can view the deposition of each  
 116 particle as a random process, and each area element on the bed surface can be assigned a probability  
 117 for the deposition of a particle. When assuming that a given number of particles are distributed on  
 118 the bed, the mean behavior of the exposed area  $A^*$  can be calculated from the following equation:  
 119

$$dA^* = -P(A^*, M_s^*, \dots) dM_s^*$$

120 (eq. 3)

121 ~~Here,~~  $P$  is the probability that a given particle is deposited on the exposed part of the bed, which  
 122 ~~here is may be~~ a function of the fraction of exposed area ( $A^*$ ) and a dimensionless mass of particles  
 123 ~~on the bed per area ( $M_s^*$ , explained below), but which may in reality can be expected to also be a~~  
 124 ~~function of~~ the relative sediment supply, the bed topography and roughness, the particle size, the  
 125 local hydraulics or other control variables.  $M_s^*$  is a dimensionless mass equal to the total mass of the  
 126 particles residing on the bed per area, which is suitably normalized. A suitable mass for normalization  
 127 is the minimum mass required to cover a unit area,  $M_0$ , as will become clear later. The minus sign is  
 128 introduced because the fraction of the exposed area reduces as  $M_s^*$  increases. Similar to eq. (3), the  
 129 equation for the fraction of covered area  $A_c^* = 1 - A^*$  can be written as:  
 130

$$dA_c^* = P(A^*, M_s^*, \dots) dM_s^*$$

131 (eq. 4)

132 As most previous relationships are expressed in terms of relative sediment supply  $Q_s^*$ , the relation of  
 133  $M_s^*$  to  $Q_s^*$  will be discussed later.

134  
 135 We can make some general statements about  $P$ . First,  $P$  is defined for the range  $0 \leq A^* \leq 1$  and  
 136 undefined elsewhere. Second,  $P$  takes values between zero and one for  $0 \leq A^* \leq 1$ . Third,  $P(A^*=0) = 0$   
 137 and  $P(A^*=1) = 1$ . Note that  $P$  is not a distribution function and therefore does not need to integrate  
 138 to one. Neither does it have to be continuous and differentiable everywhere.  
 139

140 For purpose of illustration, we will next discuss two simple forms of the probability function  $P$  that  
 141 lead to the linear and exponential forms of the cover effect, respectively. First, consider the case that  
 142 all particles are always deposited on exposed bedrock. In this case, formally, to keep with the  
 143 conditions stated above, we define  $P = 1$  for  $0 < A^* \leq 1$  and  $P = 0$  for  $A^* = 0$ . Thus, we can write  
 144

$$\begin{aligned} dA^* &= -dM_s^* & \text{for } 0 < A^* \leq 1 \\ dA^* &= 0 & \text{for } A^* = 0 \end{aligned}$$

145 (eq. 5)

146 Integrating, we obtain:

$$A^* = -M_s^* + C$$

147 (eq. 6)

148 where the constant of integration  $C$  is found to equal one by using the condition  $A^*(M_s^*=0) = 1$ . Thus,  
 149 we obtain the linear cover function of eq. (1). Note that the linear cover function gives a theoretical  
 150 lower bound for the amount of cover: it arises when all available sediment always falls on uncovered  
 151 ground, and thus no additional sediment is available that could facilitate quicker alluviation. In  
 152 essence, this is a mass conservation argument. Now it is obvious why  $M_0$  is a convenient way to  
 153 normalize: in plots of  $A^*$  against  $M_s^*$ , we obtain a triangular region bounded by the points [0,1], [0,0]  
 154 and [1,0] in which the cover function cannot exist (Fig. 1).  
 155

156 Similarly to above, if we set  $P$  to a constant value smaller than one for  $0 < A^* \leq 1$ ,  $k$ , we obtain  
 157

$$A^* = 1 - kM_s^*$$

158 (eq. 7)

159 It is clear that the assumption of  $P = k$  is physically unrealistic, because it implies that the probability  
 160 of deposition on exposed ground is independent of the amount of uncovered bedrock. Especially  
 161 when  $A^*$  is close to zero, it seems unlikely that, say, always 90% of the sediment falls on uncovered  
 162 ground. A more realistic assumption is that the probability of deposition on uncovered ground is  
 163 independent of location and other possible controls, but is equal to the fraction of exposed area, i.e.,  
 164  $P = A^*$ . In a probabilistic sense, this is also the simplest plausible assumption one can make. Then  
 165

$$dA^* = -A^* dM_s^*$$

166 (eq. 8)

167 giving upon integration

$$A^* = e^{-M_s^*}$$

168 (eq. 9)

169 The argument used here to obtain the exponential cover effect in eq. (9) essentially corresponds to  
 170 the one given by Turowski et al. (2007). Since this case presents the simplest plausible assumption,  
 171 we will use it as a benchmark case, to which we will compare other possible functional forms of  $P$ .  
 172

173 In principle, the probability function  $P$  can be varied to account for various processes that make  
 174 deposition more likely either on already covered ground by decreasing  $P$  for the appropriate range of  
 175  $A^*$  from the benchmark case  $P = A^*$ , or on uncovered ground by increasing  $P$  from the benchmark  
 176 case  $P = A^*$ . As has been identified previously (Chatanantavet and Parker, 2008; Hodge and Hoey  
 177 2012), roughness feedbacks to the flow can cause either case depending on whether subsequent  
 178 deposition is adjacent to or on top of existing sediment patches. In the former case, particles residing  
 179 on an otherwise bare bedrock bed act as obstacles for moving particles, and create a low-velocity  
 180 wake zone in the downstream direction. In addition, particles residing on other single particles are  
 181 unstable and stacks of particles are unlikely. Hence, newly arriving particles tend to deposit either  
 182 upstream or downstream of stationary particles and the probability is generally higher for deposition

183 on uncovered ground than in the benchmark case. In the latter case, larger patches of stationary  
 184 particles increase the surface roughness of the bed, thus decreasing the local flow velocity and  
 185 stresses, making deposition on the patch more likely. In this way, the probability of deposition on  
 186 already covered bed is increased in comparison to the benchmark case.

187  
 188 A simple functional form that can be used to take into account either one of these two effects is a  
 189 power law dependence of  $P$  on  $A^*$ , taking the form  $P = A^{*\alpha}$  (Fig. 1A). Then, the cover function  
 190 becomes (Fig. 1B):

$$A^* = (1 - (1 - \alpha)M_s^*)^{\frac{1}{1-\alpha}}$$

192 (eq. 10)

193 Here, the probability of deposition on uncovered ground is increased in comparison to the  
 194 benchmark exponential case if  $0 < \alpha < 1$ , and decreased if  $\alpha > 1$ .

195  
 196 A convenient and flexible way to parameterize  $P(A^*)$  in general is the cumulative version of the Beta  
 197 distribution, given by:

$$P(A^*) = B(A^*; a, b)$$

198 (eq. 11)

199 Here,  $B(A^*; a, b)$  is the regularized incomplete Beta function with two shape parameters  $a$  and  $b$ ,  
 200 which are both real positive numbers, defined by:

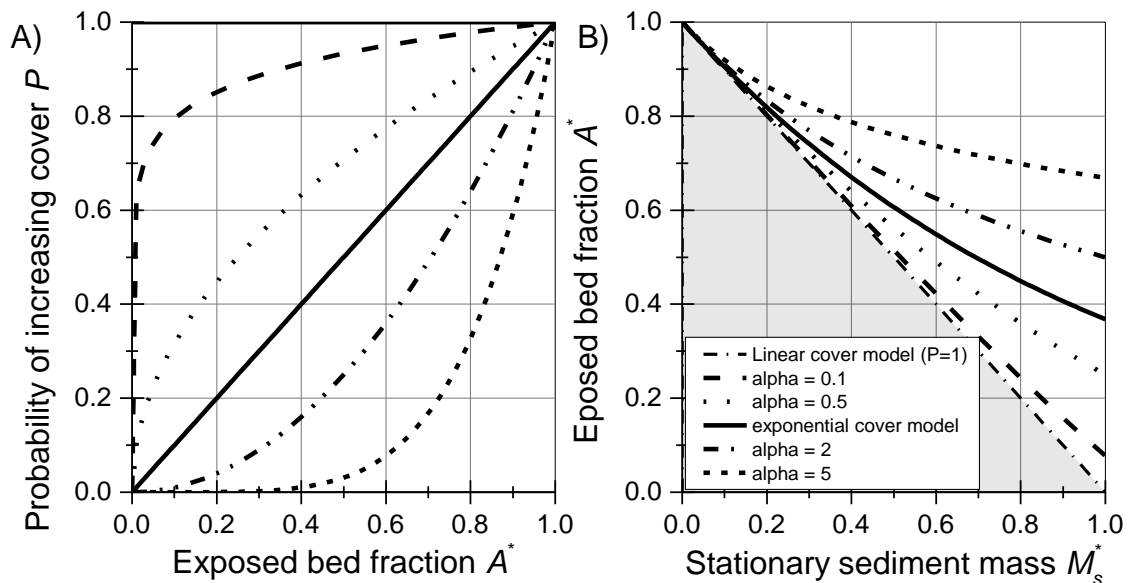
$$B(A^*; a, b) = \frac{\int_0^{A^*} y^{a-1}(1-y)^{b-1} dy}{\int_0^1 y^{a-1}(1-y)^{b-1} dy}$$

201 (eq. 12)

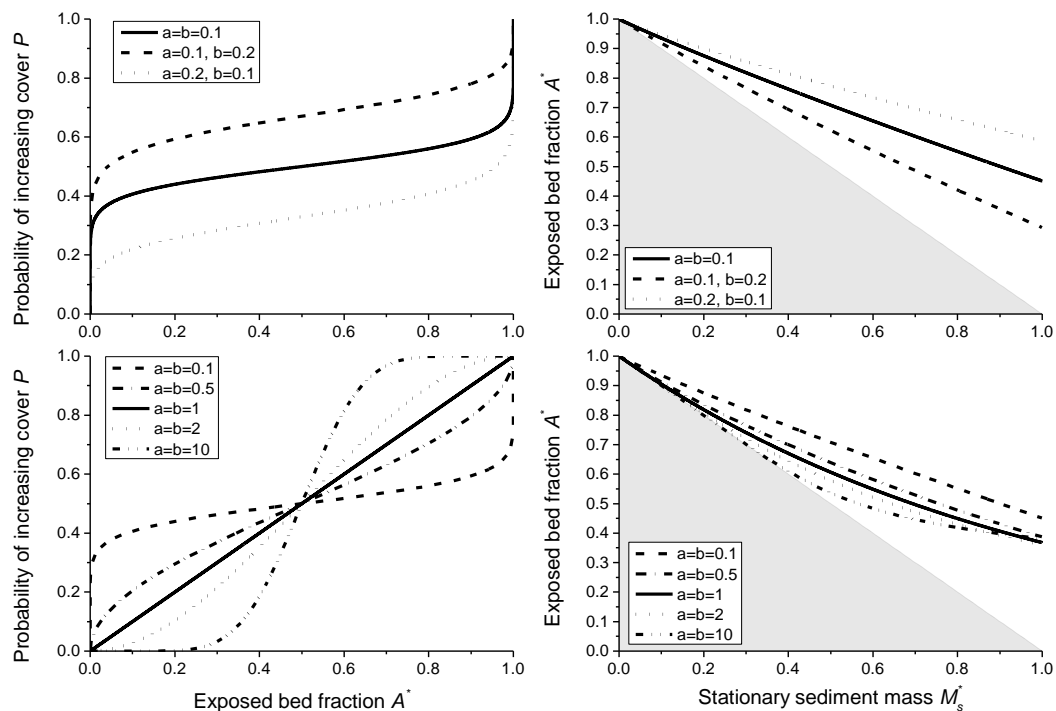
202 Here,  $y$  is a dummy variable. With suitable choices for  $a$  and  $b$ , cover functions resembling the  
 203 exponential ( $a=b=1$ ), the linear form ( $a=0, b>0$ ), and the power law form ( $a \gg b$  or  $a \ll b$ ) can be  
 204 retrieved. Wavy functions are also a possibility (Fig. 2), thus both of the roughness effects described  
 205 above can be modelled in a single scenario. Unfortunately, the integral necessary to obtain  $A^*(M_s^*)$   
 206 does not give a closed-form analytical solution and needs to be computed numerically.

207  
 208 In principle, a suitable function  $P$  could also be defined to account for the influence of bed  
 209 topography on sediment deposition. Such a function is likely dependent on the details of the  
 210 particular bed, hydraulics and sediment flow paths in a complex way and needs to be mapped out  
 211 experimentally.

212



213  
 214 Fig. 1: A) Various examples for the probability function  $P$  as a function of bedrock exposure  $A^*$ . B)  
 215 Corresponding analytical solutions for the cover function between  $A^*$  and dimensionless sediment  
 216 mass  $M_s^*$  using eq. (7), (9) and (10). Grey shading depicts the area where the cover function cannot  
 217 run due to conservation of mass.  
 218



219  
 220 Fig. 2: Examples for the use of the regularized incomplete Beta function (eq. 12) to parameterize  $P$ ,  
 221 using various values for the shape parameters  $a$  and  $b$ . The choice  $a = b = 1$  gives a dependence that  
 222 is equivalent to the exponential cover function. Grey shading depicts the area where the cover  
 223 function cannot run due to conservation of mass.  
 224

## 2.2 Example of application using model data

225

226

227 To illustrate how the framework can be used, we apply it to data obtained from the CA model  
228 developed by Hodge and Hoey (2012). The CA model reproduces the transport of individual sediment  
229 grains over a [smooth](#) bedrock surface. In each time step, the probability of a grain being entrained is  
230 a function of the number of neighboring grains. If five or more of the eight neighbouring cells contain  
231 grains then the grain has probability of entrainment  $P_e p_c$ , otherwise it has probability  $P_i p_i$ . In most  
232 model runs  $P_e p_c$  was set to a value is less than [that of  \$P\_i p\_i\$](#) , thus accounting for the impact of  
233 sediment cover in decreasing local shear stress (though increased flow resistance) and increasing the  
234 critical entrainment shear stress for grains (via lower grain exposure and increased pivot angles).  
235 [Thus, in the model, grain scale dynamics of entrainment are varied by adjusting the values of  \$p\_i\$  and](#)  
236  [\$p\_c\$ . This has a direct effect on the reach-scale distribution of cover, which is captured by our  \$P\$ -](#)  
237 [function \(eq. 3\).](#)

238

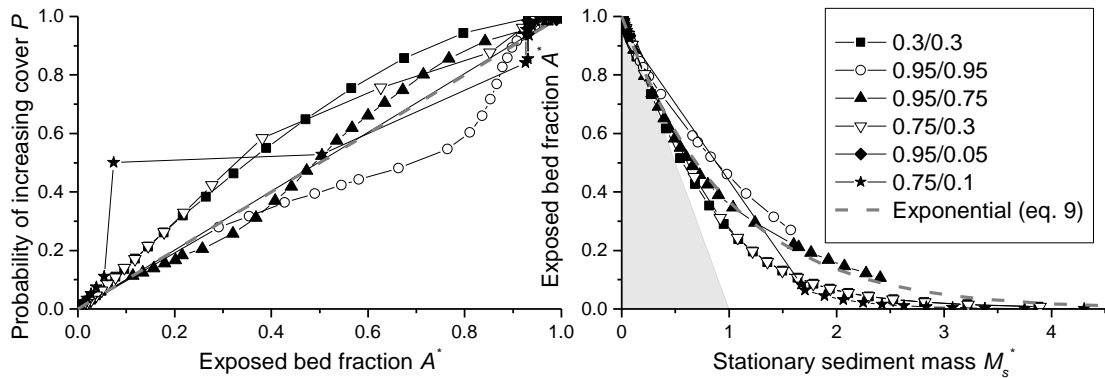
239 The model is run with a domain that is 100 cells wide by 1000 cells long, with each cell having the  
240 same area as a grain. Up to four grains can potentially be entrained from each cell in a time step,  
241 limiting the maximum sediment flux. In each time step random numbers and the probabilities are  
242 used to select the grains that are entrained, which are then moved a step length downstream. A  
243 fixed number of grains are also supplied to the upstream end of the model domain. A smoothing  
244 algorithm is applied to prevent [unrealistically local-excessively](#) tall piles of grains [developing in cells if](#)  
245 [there are far fewer grains in adjacent cells](#). After around 500 time steps the model typically reaches a  
246 steady state condition in which the number of grains supplied to and leaving the model domain are  
247 equal. Sediment cover is measured in a downstream area of the model domain and is defined as  
248 grains that are not entrained in a given time step. [Consequently grains that are deposited in one time](#)  
249 [step, and entrained in the following one do not contribute to the sediment cover, and so the model](#)  
250 [implicitly incorporates the effect of local sediment cover on grain deposition.](#)

251

252 Model runs were completed with a six different combinations of  $P_i p_i$  and  $P_e p_c$ : 0.95/0.95, 0.95/0.75,  
253 0.75/0.10, 0.75/0.30, 0.30/0.30 and 0.95/0.05. These combinations were selected to cover the range  
254 of relationships between relative sediment supply  $Q_s^*$  and the exposed bed fraction  $A^*$  observed by  
255 Hodge and Hoey (2012). For each pair of  $P_i$  and  $P_c$  model runs were completed at least 20 different  
256 values of  $Q_s^*$  in order to quantify the model behaviour.

257

258 Cover bed fraction and total mass on the bed given out by the model were converted using eq. (3)  
259 into the probabilistic framework (Fig. 3). The derivative was approximated by simple linear finite  
260 differences, which, in the case of run-away alluviation, resulted in a non-continuous curve due to  
261 large gradients. The exponential benchmark (eq. 9) is also shown for comparison. The different  
262 model parameterisations produce results in which the probability of deposition on bedrock is both  
263 more and less likely than in the baseline case, with some runs showing both behaviours. Cases where  
264 the probability is more than the baseline case (i.e. grains are more likely to fall on uncovered areas)  
265 are associated with runs in which grains in clusters are relatively immobile. These runs are likely to be  
266 particularly affected by the smoothing algorithm that acts to move sediment from alluviated to  
267 bedrock areas. All model parameterisations predict greater bed exposure for a given normalised  
268 mass than is predicted by a linear cover relationship (Figure 3b). Runs with relatively more immobile  
269 cluster grains have a lower exposed fraction for the same normalised mass. Runs with low values of  
270  $P_i p_i$  and  $P_e p_c$  seem to lead to behavior in which cover is more likely than in the exponential  
271 benchmark, while for high values, it is less likely. However, there are complex interactions and  
272 general statements cannot be made straightforwardly.



274

275

276

277

278

279

280

281

282

283

284

285

286

287

288

289

290

291

292

293

294

295

296

297

298

299

300

301

302

303

304

305

306

307

308

309

Fig. 3: Probability functions  $P$  and cover function derived from data obtained from the model of Hodge and Hoey (2012). The grey dashed line shows the exponential benchmark behavior. Grey shading depicts the area where the cover function cannot run due to conservation of mass. The legend gives values of the probabilities of entrainment  $P_e - p_e$  and  $P_c - p_c$  used for the runs (see text).

### 3. Cover development in time and space

#### 3.1. Model derivation

Previous descriptions of the cover effect relate the exposed fraction of the bed to the relative sediment supply  $Q_s^*$  (see eqs. 1 and 2). The relation between  $Q_s^*$  and  $M_s$ , which we used in eq. (3), has often been muddled and incorrect (see, for example, Turowski et al., 2007). In this chapter, we derive a model to clarify this relationship and put it on a sound physical bases. To this end, the probabilistic formulation introduced above can be extended to allow the calculation of the temporal and spatial evolution of sediment cover in a stream. Here, we will derive the equations for the one dimensional case (linear flume), but extensions to higher dimensions are possible in principle. The derivation is inspired by the erosion-deposition framework (e.g. Charru et al., 2004; Turowski, 2009), with some necessary adaptations to make it suitable for channels with partial sediment cover. In our system, we consider two separate mass reservoirs within a control volume. The first reservoir contains all particles in motion, the total mass per bed area of which is denoted by  $M_m$ , while the second reservoir contains all particles that are stationary on the bed, the total mass per bed area of which is denoted by  $M_s$ . We need then three further equations, one to connect the rate of change of mobile mass to the sediment flux in the flume, one to govern the exchange of particles between the two reservoirs, and one to describe how sediment transport rate is related to the mobile mass. The first of these is of course the Exner equation of sediment continuity (e.g. Paola and Voller, 2005), which captures mass conservation in the system. Instead of the common approach tracking the height of the sediment over a reference level, we use the total sediment mass on the bed as a variable, giving

$$\frac{\partial M_m}{\partial t} = -\frac{\partial q_s}{\partial x} + E - D$$

(eq. 13)

Here,  $x$  is the coordinate in the streamwise direction,  $t$  the time,  $q_s$  the sediment mass transport rate per unit width, while  $E$  is the mass entrainment rate per bed area and  $D$  is the mass deposition rate per bed area. The latter two terms give the flux describe the exchange of particles between reservoirs; in the single reservoir Exner equation these terms are not needed. It is clear that for the

310 problem at hand the choice of total mass or volume as a variable to track the amount of sediment in  
 311 the reach of interest is preferable to the height of the alluvial cover, since necessarily, when cover is  
 312 patchy, the height of the alluvium varies across the bed. It is useful to work with dimensionless  
 313 variables by defining  $t^* = t/T$  and  $x^* = x/L$ , where  $T$  and  $L$  are suitable time and length scales,  
 314 respectively. The dimensionless mobile mass per bed area  $M_m^*$  is equal to  $M_m/M_0$ , and eq. (13)  
 315 becomes:

$$\frac{\partial M_m^*}{\partial t^*} = -\frac{\partial q_s^*}{\partial x^*} + E^* - D^*$$

317 (eq. 14)

318 Here,

$$q_s^* = \frac{T}{LM_0} q_s$$

319 (eq. 15)

320 The dimensionless entrainment and deposition rates,  $E^*$  and  $D^*$ , are equal to  $TE/M_0$  and  $TD/M_0$ ,  
 321 respectively. The rate of change of the stationary sediment mass  $M_s$  in time is the difference of the  
 322 deposition rate  $D$  and the entrainment rate  $E$ :

$$\frac{\partial M_s}{\partial t} = D - E$$

324 (eq. 16)

325 Or, using dimensionless variables

$$\frac{\partial M_s^*}{\partial t^*} = D^* - E^*$$

326 (eq. 17)

327 We also need sediment entrainment and deposition functions. The entrainment rate needs to be  
 328 modulated by the availability of sediment on the bed. If  $M_s^*$  is equal to zero, no material can be  
 329 entrained. A plausible assumption is that the maximal entrainment rate,  $E_{max}^*$ , is equal to the  
 330 transport capacity.

$$E_{max}^* = q_t^*$$

331 (eq. 18)

332 Here,  $q_t^*$  is the dimensionless mass transport capacity, which is related to the transport capacity per  
 333 unit width  $q_t$  by a relation similar to eq. (15). To first order, the rate of change in entrainment rate,  
 334  $dE$ , is proportional to the difference of  $E_{max}$  and  $E$ , and to the rate of change in mass on the bed.

335

$$dE^* = (E_{max}^* - E^*)dM_s^* = (q_t^* - E^*)dM_s^*$$

336 (eq. 19)

337 Integrating, we obtain

338

$$E^* = E_{max}^*(1 - e^{-M_s^*}) = (1 - e^{-M_s^*})q_t^*$$

339 (eq. 20)

340 Here, we used the condition  $E^*(M_s^*=0) = 0$  to fix the integration constant to  $E_{max}^*$ . As required, eq.  
 341 (20) approaches  $E_{max}^*$  as  $M_s^*$  goes to infinity, and is equal to zero when  $M_s^*$  is equal to zero. Using a  
 342 similar line of argument, and by assuming the maximum deposition rate to be equal to  $q_s^*$ , we arrive  
 343 at an equation for the deposition rate  $D^*$ .

344

$$D^* = (1 - e^{-M_m^*})q_s^*$$

345 (eq. 21)



346 | [When  \$M\_m^\*\$  is small, then the amount that can be deposited is limited by  \$M\_m^\*\$ . If  \$M\_m^\*\$  is large, then](#)  
 347 | [deposition is limited by sediment supply.](#) Substituting eqs. (20) and (21) into eq. (17), we obtain:  
 348

$$\frac{\partial M_s^*(x^*, t^*)}{\partial t^*} = D^* - E^* = (1 - e^{-M_m^*(x^*, t^*)})q_s^*(x^*, t^*) - (1 - e^{-M_s^*(x^*, t^*)})q_t^*(x^*, t^*)$$

349 (eq. 22)

350 Note that  $q_s^*/q_t^* = Q_s^*$ . The equation for the mobile mass (eq. 14) becomes:

351

$$\frac{\partial M_m^*(x^*, t^*)}{\partial t^*} = -\frac{\partial q_s^*}{\partial x^*} - (1 - e^{-M_m^*(x^*, t^*)})q_s^*(x^*, t^*) + (1 - e^{-M_s^*(x^*, t^*)})q_t^*(x^*, t^*)$$

352 (eq. 23)

353 Finally, the sediment transport rate needs to be proportional to the mobile sediment mass times the  
 354 downstream sediment speed  $U$ , and we can write

355

$$q_s^*(x^*, t^*) = U^*(x^*, t^*)M_m^*(x^*, t^*)$$

356 (eq. 24)

357 Here

$$U^* = \frac{T}{L}U$$

358 (eq. 25)

359

360 After incorporating the original equation between  $A^*$  and  $M_s^*$  (eq. 3), the system of four differential  
 361 equations (3), (22), (23) and (24) contains four unknowns: the downstream gradient in the sediment  
 362 transport rate  $\partial q_s^*/\partial x^*$ , the exposed fraction of the bed  $A^*$ , the non-dimensional stationary mass  $M_s^*$ ,  
 363 and the non-dimensional mobile mass  $M_m^*$ , while the non-dimensional transport capacity  $q_t^*$  and the  
 364 non-dimensional downstream sediment speed  $U^*$  are input variables, and  $P$  is a externally specified  
 365 function. In addition, sediment input  $q_s^*$  needs to be specified as an upstream boundary condition  
 366 and initial values for the mobile mass  $M_m^*$  and the stationary mass  $M_s^*$  need to be specified  
 367 everywhere.

368

### 369 3.2. Time-independent solution

370

371 Setting the time derivatives to zero, we obtain a time-independent solution, which links the exposed  
 372 area directly to the ratio of sediment transport rate to transport capacity. From eq. (23) it follows  
 373 that in this case, the entrainment rate is equal to the deposition rate and we obtain

$$(1 - e^{-\overline{M_m^*}})\overline{q_s^*} = (1 - e^{-\overline{M_s^*}})q_t^*$$

374 (eq. 26)

375 Here, the bar over the variables denotes their steady state value. Substituting eq. (24) to eliminate  
 376  $\overline{M_m^*}$  and solving for  $\overline{M_s^*}$  gives

377

$$\overline{M_s^*} = -\ln \left\{ 1 - \left( 1 - e^{-\frac{\overline{q_s^*}}{U^*}} \right) \frac{\overline{q_s^*}}{q_t^*} \right\} = -\ln \left\{ 1 - \left( 1 - e^{-\frac{q_t^* \overline{Q_s^*}}{U^*}} \right) \overline{Q_s^*} \right\}$$

378 (eq. 27)

379 Note that we assume here that sediment cover is only dependent on the stationary sediment mass  
 380 on the bed and we thus neglect grain-grain interactions known as the dynamic cover (Turowski et al.,  
 381 2007). In analogy to eq. (24), we can write

$$q_t^* = U^* M_0^*$$

382 (eq. 28)

383 Here,  $M_0^*$  is a characteristic dimensionless mass that depends on hydraulics and therefore implicitly  
 384 on transport capacity (which is independent of and should not be confused with the minimum mass  
 385 necessary to fully cover the bed  $M_0$ ). When sediment transport rate equals transport capacity, then  
 386  $M_0^*$  is equal to the mobile mass of sediment normalized by the reference mass  $M_0$ . It can be viewed  
 387 as a proxy for the transport capacity and is a convenient parameter to simplify the equations. The  
 388 mobile mass can then, in general, be written as [follows](#) (cf. Turowski et al., 2007), remembering that  
 389 the relative sediment supply  $Q_s^* = 1$  when supply is equal to capacity:

$$M_m^* = M_0^* Q_s^*$$

390 (eq. 29)

391 If we use the exponential cover function (eq. 9) with eqs. (27), (28) and (29) we obtain

392

$$\bar{A}^* = 1 - \left( 1 - e^{-\frac{\bar{q}_s^*}{U^*}} \right) \frac{\bar{q}_s^*}{q_t^*} = 1 - \left( 1 - e^{-\frac{q_t^* \bar{Q}_s^*}{U^*}} \right) \bar{Q}_s^* = 1 - \left( 1 - e^{-M_0^* \bar{Q}_s^*} \right) \bar{Q}_s^*$$

393 (eq. 30)

394 Similarly, equations can be found for the other analytical solutions of the cover function. For the  
 395 linear case (eq. 7), we obtain:

$$\bar{A}^* = 1 + \ln \left\{ 1 - \left( 1 - e^{-M_0^* \bar{Q}_s^*} \right) \bar{Q}_s^* \right\}$$

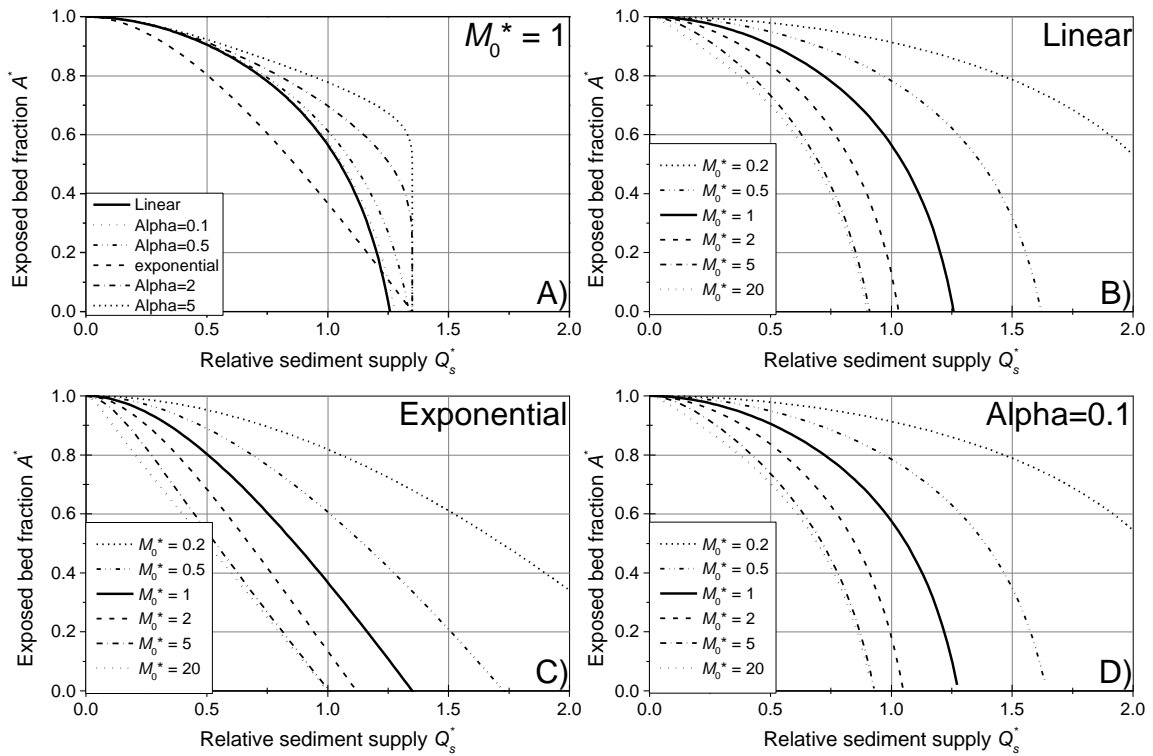
396 (eq. 31)

397 For the power law case (eq. 10), we obtain:

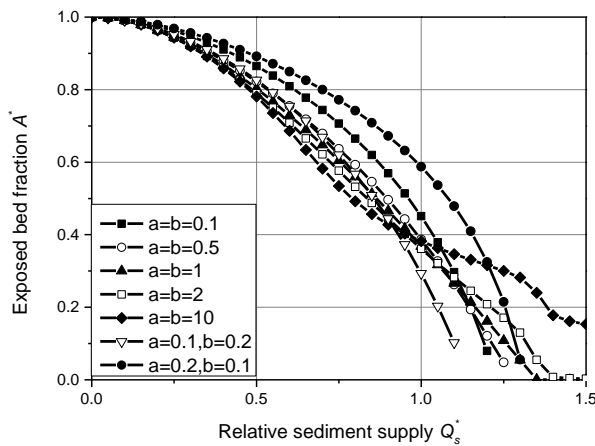
$$\bar{A}^* = \left[ 1 + (1 - \alpha) \ln \left\{ 1 - \left( 1 - e^{-M_0^* \bar{Q}_s^*} \right) \bar{Q}_s^* \right\} \right]^{\frac{1}{1-\alpha}}$$

398 (eq. 32)

399 It is interesting that the assumption of an exponential cover function essentially leads to a combined  
 400 linear and exponential relation between  $\bar{A}^*$  and  $\bar{Q}_s^*$ . Instead of a linear decline as the original linear  
 401 cover model, or a concave-up relationship as the original exponential model, the function is convex-  
 402 up for all solutions (Fig. 4). Adjusting  $M_0^*$  shifts the lines: decreasing  $M_0^*$  leads to a delayed onset of  
 403 cover and vice versa. The former result arises because a lower  $M_0^*$  means that the sediment flux is  
 404 conveyed through a smaller mass moving at a higher velocity. The original linear cover function (eq.  
 405 1) can be recovered from the exponential model with a high value of  $M_0^*$ , since the exponential term  
 406 quickly becomes negligible with increasing  $\bar{Q}_s^*$  and the linear term dominates (Fig. 4C). Note that for  
 407 the linear (eq. 6) and the power law cases (eq. 10), high values of  $M_0^*$  may give  $\bar{A}^* = 0$  for  $\bar{Q}_s^* < 1$  (Fig.  
 408 4B,D), which is consistent with the concept of runaway alluviation. Using the beta distribution to  
 409 describe  $P$ , a numerical solution is necessary, but a wide range of steady-state cover functions can be  
 410 obtained (Fig. 5). By varying the value of  $M_0^*$ , an even wider range of behavior can be obtained.



411  
 412 Fig. 4: Analytical solutions at steady state for the exposed fraction of the bed ( $A^*$ ) as a function of  
 413 relative sediment supply ( $Q_s^*$ , cf. Fig. 1). A) Comparison of the different solutions, keeping  $M_0^*$   
 414 constant at 1. B) Varying  $M_0^*$  for the linear case (eq. 31). C) Varying  $M_0^*$  for the exponential case (eq.  
 415 30). D) Varying  $M_0^*$  for the power law case with  $\alpha = 0.1$  (eq. 32).  
 416



417  
 418 Fig. 5: Steady state solutions using the beta distribution to parameterize  $P$  (eq. 11) for a range of  
 419 parameters  $a$  and  $b$ , and using  $M_0^* = 1$  (cf. Fig. 2). The solutions were obtained by iterating the  
 420 equations to a steady state, using initial conditions of  $A^* = 1$  and  $M_m^* = M_s^* = 0$ .  
 421

422 The previous analysis shows that steady state cover is controlled by the characteristic dimensionless  
 423 mass  $M_0^*$ , which is equal to the ratio of dimensionless transport capacity and particle speed (eq. 28).  
 424 Converting to dimensional variables, we can write

$$M_0^* = \frac{q_t^*}{U^*} = \frac{q_t}{M_0 U}$$

425 (eq. 33)

426 The minimum mass necessary to completely cover the bed per unit area,  $M_0$ , can be estimated  
 427 assuming a single layer of close-packed spherical grains residing on the bed (cf. Turowski, 2009),  
 428 giving:

$$M_0 = \frac{\pi \rho_s D_{50}}{3\sqrt{3}}$$

429 (eq. 34)

430 Here,  $\rho_s$  is the sediment density and  $D_{50}$  is the median grain size. [We use equations derived by](#)  
 431 [Fernandez-Luque and van Beek \(1976\) derived equations both from flume experiments that describe](#)  
 432 [for the transport capacity and the particle speed from flume experiments, using as a function of](#) bed  
 433 shear stress [as a control parameter](#) (see also Lajeunesse et al., 2010, and Meyer-Peter and Mueller,  
 434 1948, for similar equations):

435

$$q_t = 5.7 \frac{\rho_s \rho}{(\rho_s - \rho) g} \left( \frac{\tau}{\rho} - \frac{\tau_c}{\rho} \right)^{3/2}$$

436 (eq. 35)

437

$$U = 11.5 \left( \left( \frac{\tau}{\rho} \right)^{1/2} - 0.7 \left( \frac{\tau_c}{\rho} \right)^{1/2} \right)$$

438 (eq. 36)

439 Here,  $\tau_c$  is the critical bed shear stress for the onset of bedload motion,  $g$  is the acceleration due to  
 440 gravity and  $\rho$  is the water density. Combining eqs. (34), (35) and (36) to get an equation for  $M_0^*$  gives:

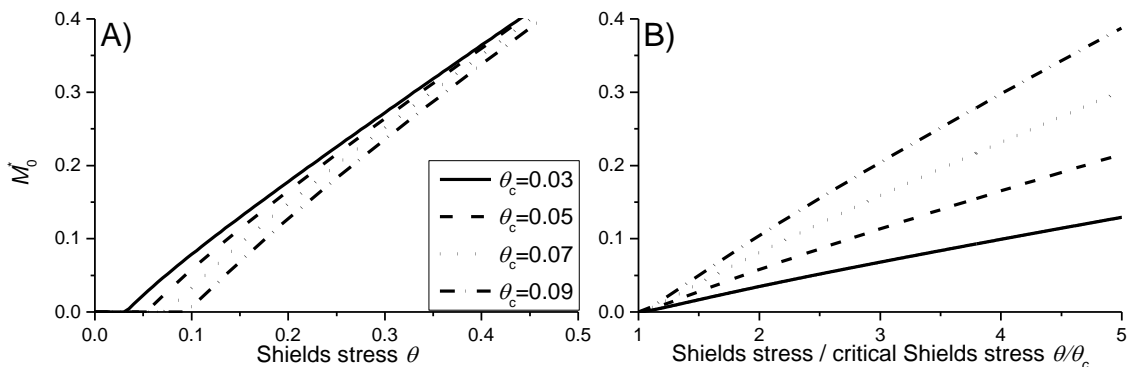
441

$$M_0^* = \frac{3\sqrt{3}}{2\pi} \frac{(\theta - \theta_c)^{3/2}}{\theta^{1/2} - 0.7\theta_c^{1/2}} = \frac{3\sqrt{3}\theta_c}{2\pi} \frac{(\theta/\theta_c - 1)^{3/2}}{(\theta/\theta_c)^{1/2} - 0.7}$$

442 (eq. 37)

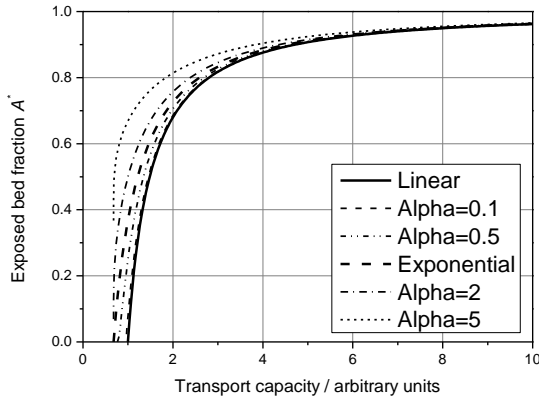
443 Here, the Shields stress  $\theta = \tau/(\rho_s - \rho)gD_{50}$ , and  $\theta_c$  is the corresponding critical Shields stress, and we  
 444 approximated  $5.7/11.5 = 0.496$  with  $1/2$  (compare to eqs. 35/36). At high  $\theta$ , when the threshold can  
 445 be neglected, eq. (37) reduces to a linear relationship between  $M_0^*$  and  $\theta$ . Near the threshold,  $M_0^*$   
 446 is shifted to lower values as  $\theta_c$  increases (Fig. 6). The systematic variation of  $U^*$  with the hydraulic  
 447 driving conditions (eq. 36) implies that the cover function evolves differently in response to changes  
 448 in sediment supply and transport capacity. For a first impression, by comparing equations (35) and  
 449 (36), we assume that particle speed scales with transport capacity raised to the power of one third  
 450 (Fig. 7).

451



452

453 Fig. 6: The characteristic dimensionless mass  $M_0^*$  depicted as a function of A) the Shields stress and  
 454 B) the ratio of Shields stress to critical Shields stress (eq. 37).  
 455



456  
 457 Fig. 7: Variation of the exposed bed fraction as a function of transport capacity, assuming that  
 458 particle speed scales with transport capacity to the power of one third.  
 459

### 460 3.3 Temporal evolution of cover within a reach

#### 461 3.3.1 System timescales

462 To calculate the temporal evolution of cover on the bed within a single reach, we solved the  
 463 equations numerically for a section of the bed with homogenous conditions using a simple linear  
 464 finite difference scheme. Then, the sediment input is a boundary condition, while sediment output,  
 465 mobile and stationary sediment mass and the fraction of the exposed bed are output variables. In  
 466 general, a change in sediment supply leads to a gradual adjustment of the output variables towards a  
 467 new steady state (Fig. 8). Unfortunately, a general analytical solution is not possible, but a results can  
 468 be obtained for the special case of  $q_s^* = 0$ . Such a situation is rare in nature, but could be easily  
 469 created in flume experiments as a model test. Then, the time derivative of stationary mass is given  
 470 by:

$$471 \frac{\partial M_s^*}{\partial t^*} = -(1 - e^{-M_s^*})q_t^*$$

472 (eq. 38)

473 Using the exponential cover model (eq. 9), we obtain:

474

$$\frac{1}{A^*(1 - A^*)} \frac{\partial A^*}{\partial t^*} = q_t^*$$

475 (eq. 39)

476 Equation (39) is separable and can be integrated to obtain

477

$$\ln(A^*) - \ln(1 - A^*) = t^*q_t^* + C$$

478 (eq. 40)

479 Letting  $A^*(t^*=0) = A_0^*$ , where  $A_0^*$  is the initial cover, the final equation is

480

$$\frac{1 - A^* A_0^*}{1 - A_0^* A^*} = e^{-t^*q_t^*}$$

481 (eq. 41)

482 To clarify the characteristic time scale of the process, equation (41) can also be written in the form of  
 483 a sigmoidal-type function:

484

$$A^* = \frac{1}{1 + \left(\frac{1 - A_0^*}{A_0^*}\right) e^{-t^* q_t^*}}$$

485 (eq. 42)

486 By making the parameters in the exponent on the right hand side of eq. (42) dimensional, we get:

487

$$t^* q_t^* = \frac{t}{T} \frac{T}{LM_0} q_t = \frac{t q_t}{LM_0}$$

488 (eq. 43)

489 which allows a characteristic system time scale  $T_E$  to be defined as

$$T_E = \frac{LM_0}{q_t}$$

490 (eq. 44)

491 Since this time scale is dependent on the transport capacity  $q_t$ , we can view it as a time scale  
 492 associated with the entrainment of sediment from the bed (cf. eq. 20) – hence the subscript  $E$  on  $T_E$ .  
 493 From eq. (42), the exposed bed fraction evolves in an asymptotic fashion towards equilibrium (Fig. 9).  
 494 We can expect that there are other characteristic time scales for the system, for example associated  
 495 with sediment deposition or downstream sediment evacuation.

496

497 We can make some further progress and define a more general system time scale by performing a  
 498 perturbation analysis (Appendix A). For small perturbations in either  $q_s^*$  or  $q_t^*$ , we obtain an  
 499 exponential term describing the transient evolution, which allows the definition of a system  
 500 timescale  $T_S$

$$\exp \left\{ - \left( \frac{\bar{q}_t}{\bar{q}_t} - \left( 1 - e^{-\frac{\bar{q}_s^*}{U^*}} \right) \frac{\bar{q}_s}{\bar{q}_t} \right) t^* \right\} = \exp \left\{ - \frac{t}{T_S} \right\}$$

501 (eq. 45)

502 The characteristic system time scale can then be written as

$$T_S = \frac{LM_0}{\bar{q}_t \left( 1 - \left( 1 - e^{-\frac{\bar{q}_s^*}{U^*}} \right) \frac{\bar{q}_s}{\bar{q}_t} \right)} = \frac{LM_0}{\bar{q}_t} e^{\bar{M}_s^*}$$

503 (eq. 46)

504 Note that for  $q_s^* = 0$ , eq. (46) reduces to eq. (44), as would be expected. Since  $\bar{M}_s^*$  is directly related  
 505 to steady state bed exposure  $\bar{A}^*$ , we can rewrite the equation, for example by assuming the  
 506 exponential cover function (eq. 3), as

$$T_S = \frac{LM_0}{\bar{q}_t \bar{A}^*}$$

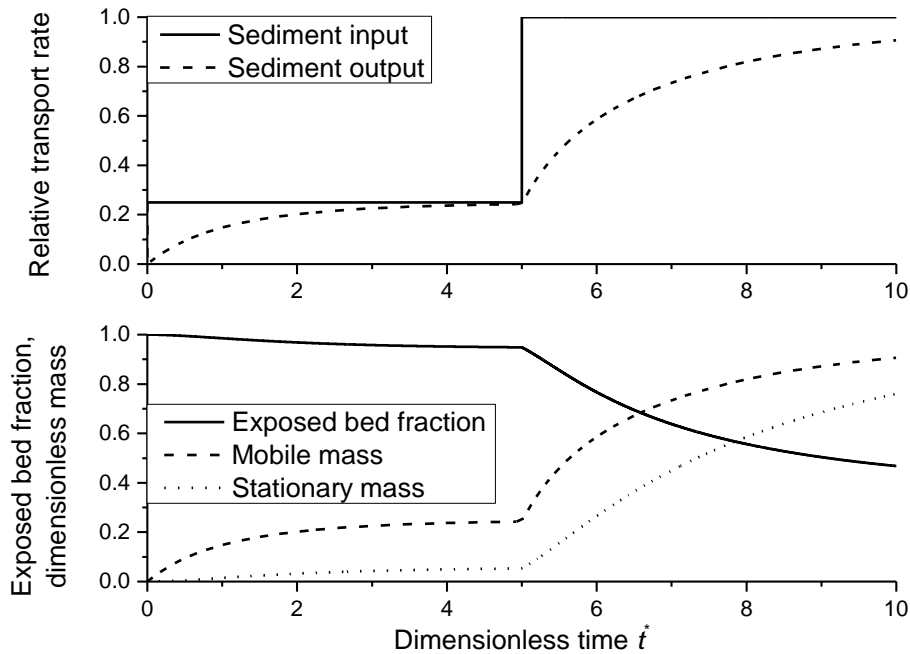
507 (eq. 47)

508 Since bed cover is more easily measurable than the mass on the bed, eq. (47) can help to estimate  
 509 system time scales in the field. Further,  $\bar{A}^*$  varies between 0 and 1, which allows estimating a  
 510 minimum system time using eq. (44). As  $\bar{A}^*$  approaches zero, the system time [scale](#) diverges.

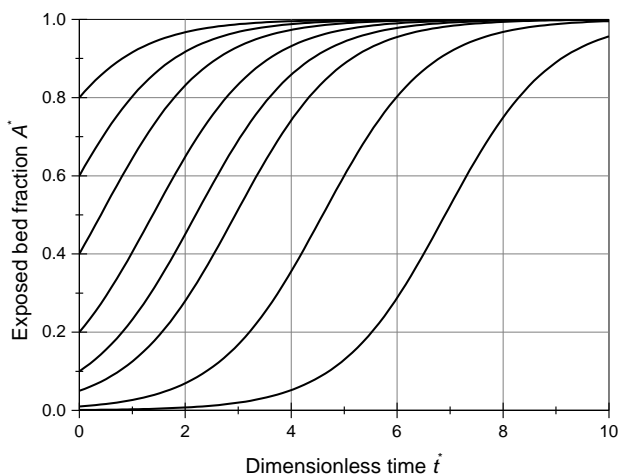
511

512 To illustrate these additional dependencies, we have [used numerical solutions of eqs. \(3\), \(22\), \(23\)](#)  
 513 [and \(24\) to calculate](#) the time needed to reach 99.9% ~~(chosen due to the asymptotic behavior of the~~

514 | system) of total adjustment after a step change in transport stage (chosen due to the asymptotic  
515 | behavior of the system), produced by varying particle speed  $U$  over a range of plausible values (Fig.  
516 | 10). Response time decreases as particle speed increases. This reflects elevated downstream  
517 | evacuation for higher particles speeds, resulting in a smaller mobile particle mass and thus higher  
518 | entrainment and lower deposition rates. Response time also increases with increasing relative  
519 | sediment supply  $Q_s^* q_s / q_c$ . As the runs start with zero sediment cover, and the extent of cover  
520 | increases with  $Q_s^* q_s / q_c$ , at higher  $Q_s^* q_s / q_c$  the adjusted cover takes longer to develop.  
521

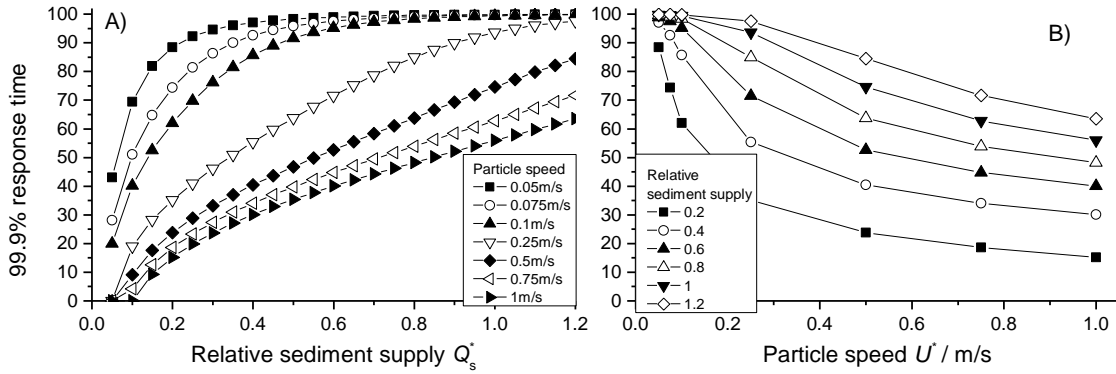


522  
523 Fig. 8: Temporal evolution of cover for the simple case of a control box with sediment through-flux,  
524 based on eqs. (3), (22), (23) and (24). Relative sediment supply (supply normalized by transport  
525 capacity) was specified to 0.25 and increased to 1 at  $t^* = 5$ . The response of sediment output, mobile  
526 and stationary sediment mass and the exposed bed fraction was calculated. Here, we used the  
527 exponential function for  $P$  (eq. 9) and  $M_0^* = U^* = 1$ . The initial values were  $A^* = 1$  and  $M_m^* = M_s^* = 0$ .  
528



529

530 Fig. 9: Evolution of the exposed bed fraction (removal of sediment cover) over time starting with  
 531 different initial values of bed exposure, for the special case of no sediment supply, i.e.,  $q_s^* = 0$  (eq. 41)  
 532 and  $q_t^* = 1$ .  
 533



534  
 535 Fig. 10: Dimensionless time to reach 99.9% of the total adjustment in exposed area as a function of  
 536 A) transport stage and B) particle speed. All simulation were started with  $A^* = 1$  and  $M_m^* = M_s^* = 0$ .  
 537

538  
 539  
 540 **3.3.2 Phase shift and gain in response to a cyclic perturbation**

541 The perturbation analysis (Appendix A) gives some insight into the response of cover to cyclic  
 542 sinusoidal perturbations. Let sediment supply be perturbed in a cyclic way described by an equation  
 543 of the form

$$q_s^* = \overline{q_s^*} + \delta q_s^* = \overline{q_s^*} + d \sin\left(\frac{2\pi t}{p}\right)$$

544 (eq. 48)

545 Here, the overbar denotes the temporal average,  $\delta q_s^*$  is the time-dependent perturbation,  $d$  is the  
 546 amplitude of the perturbation and  $p$  its period. A similar perturbation can be applied to the transport  
 547 capacity (see Appendix A). The reaction of the stationary mass and therefore cover can then also be  
 548 described by sinusoidal function of the form (Appendix A)

$$\delta M_s^* = G \sin\left(\frac{2\pi t}{p} + \varphi\right)$$

549 (eq. 49)

550 Here,  $\delta M_s^*$  is the perturbation of the stationary sediment mass around the temporal average,  $G$  is  
 551 known as the gain, describing the amplitude response, and  $\varphi$  is the phase shift. If the gain is large,  
 552 stationary mass reacts strongly to the perturbation; if it is small, the forcing does not leave a signal.  
 553 The phase shift is negative if the response lags behind the forcing and positive if it leads. The phase  
 554 shift can be written as

$$\varphi = \tan^{-1}\left(-2\pi \frac{T_s}{p}\right)$$

555 (eq. 50)

556 The gain can be written as

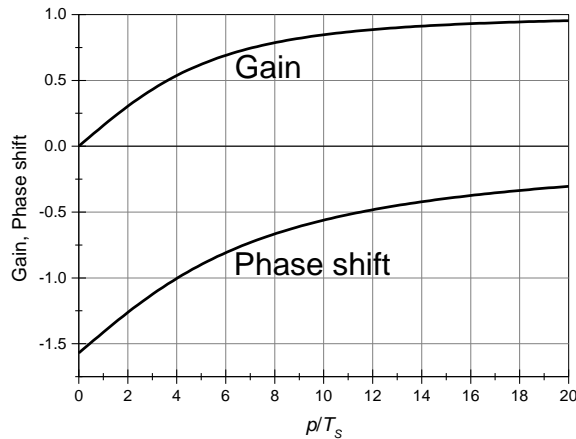
$$G = \frac{p}{T_s} \frac{Kd}{\sqrt{\left(\frac{p}{T_s}\right)^2 + 4\pi^2}}$$

557 (eq. 51)

558 Here,  $d$  is the amplitude of the perturbation, and  $K$  is a function of the time-averaged values of  $q_s$ ,  $q_t$   
 559 and  $U$  and differs for perturbations in transport capacity and sediment supply (see Appendix A).



560 Thus, the system behavior can be interpreted as a function of the ratio of the period of perturbation  
 561  $p$  and the system time scale  $T_s$ . The period  $p$  is large if the forcing parameter, i.e., discharge or  
 562 sediment supply, varies slowly and small when it varies quickly. According to eq. (50), the phase shift  
 563 is equal to  $-\pi/2$  for low values of  $p/T_s$  (quickly-varying forcing parameter), implying a substantial lag in  
 564 the adjustment of cover. The phase shift tends to zero as  $p/T_s$  tends to infinity (Fig. 11). The gain  
 565 varies approximately linearly with  $p/T_s$  for small  $p/T_s$  (quickly-varying forcing parameter), while it is  
 566 approximately constant at a value of  $Kd$  for large  $p/T_s$  (slowly-varying forcing parameter) (eq. 51).  
 567 Thus, if the forcing parameter varies slowly, cover adjustment keeps up at all times.  
 568



569 Fig. 11: Phase shift (eq. 50) and gain (eq. 51) as a function of the ratio of the period of perturbation  
 570  $p$  and the system time scale  $T_s$ . For the calculation, the constant factor in the gain ( $Kd$ ) was set  
 571 equal to one.  
 572

### 573 3.3.3 A flood at the Erlenbach

574 To illustrate the magnitude of the timescales using real data, we use a flood dataset from the  
 575 Erlenbach, a sediment transport observatory in the Swiss Prealps (e.g., Beer et al., 2015). There, near  
 576 a discharge gauge, bedload transport rates are measured at 1-minute resolution using the Swiss Plate  
 577 Geophone System, a highly developed and fully calibrated surrogate bedload measuring system (e.g.,  
 578 Rickenmann et al., 2012; Wyss et al. 2016). We use data from a flood on 20<sup>th</sup> June 2007 (Turowski et  
 579 al., 2009) with highest peak discharge that has so far been observed at the Erlenbach. The  
 580 meteorological conditions that triggered this flood and its geomorphic effects have been described in  
 581 detail elsewhere (Molnar et al., 2010; Turowski et al., 2009, 2013). ~~Although the~~ The Erlenbach does not  
 582 have a bedrock bed in the sense that bedrock is exposed in the channel bed, however, the data  
 583 provide a realistic natural time series of discharge and bedload transport over the course of a single  
 584 event. Rather than predicting bed cover evolution for a natural system, for which we do not currently  
 585 have data for validation, we use the Erlenbach data to -and are ideal for illustrating-illustrate possible  
 586 cover behavior during a fictitious event and with different initial sediment cover extents, using  
 587 natural data to provide realistic boundary conditions.  
 588

589 Using a median grain size of 80 mm, a sediment density of 2650 kg/m<sup>3</sup> and a reach length of 50 m,  
 590 we obtained  $M_0 = 128 \text{ kg/m}^2$ . We calculated transport capacity using the equation of Fernandez  
 591 Luque and van Beek (1976). However, it is known that this and similar equations strongly  
 592 overestimate measured transport rates in streams such as the Erlenbach (e.g., Nitsche et al., 2011).  
 593 Consequently, we rescaled by setting the ratio of bedload supply to capacity to one at the highest  
 594 discharge. The exposed fraction was then calculated iteratively assuming  $P = A^*$  (i.e., the exponential  
 595

596 cover formulation, eq. 9). In a real flood event, water discharge and sediment supply obviously do  
 597 not follow a small cyclic perturbation (Fig. 11). But we can tentatively relate the observations to the  
 598 theory by assuming that at each time step, [the change in sediment supply can be represented by the](#)  
 599 [commencement of](#) a sinusoidal perturbation with varying period ~~commences~~. To estimate the  
 600 [effective](#) period  $p$ , one needs to take the derivatives of eq. (48).

$$\frac{dq_s^*}{dt} = \frac{d\delta q_s^*}{dt} = \frac{2\pi d}{p} \cos\left(\frac{2\pi t}{p}\right)$$

601 (eq. 52)

602 Setting  $t = 0$  for the time of interest, we can relate  $p$  to the local gradient in bedload supply, which  
 603 can be measured from the data.

604

$$\frac{2\pi d}{p} = \frac{\Delta q_s^*}{\Delta t}$$

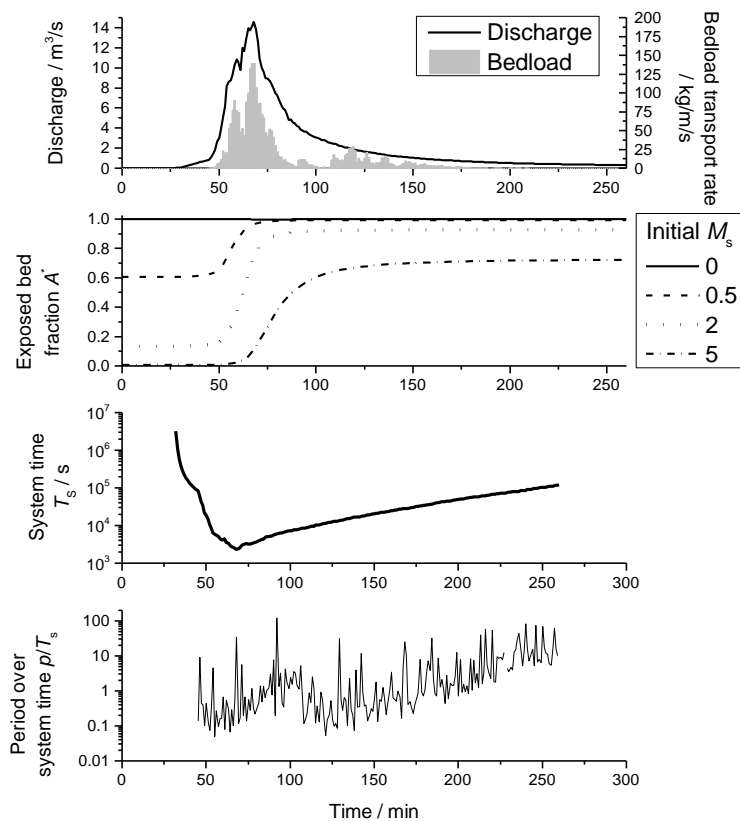
605 (eq. 52)

606 Assuming that all change in the response time is due to changes in the period (i.e., assuming a  
 607 constant amplitude,  $d = 1$ ), we can obtain a conservative estimate of the range over which  $p$  varies  
 608 over the course of an event.

$$p = 2\pi \frac{\Delta t}{\Delta q_s^*}$$

609 (eq. 52)

610 In the exemplary event, the evolution and final value of bed cover depends strongly on its initial  
 611 value (Fig. 12), indicating that the adjustment is incomplete. The system timescale is generally larger  
 612 than 1000s and is inversely related to discharge via the dependence on transport capacity. The  
 613  $p/T_s$  ratio varies around one, with low values at the beginning of the flood and large values in the  
 614 waning hydrograph. Both the high [values of the](#) system time [scale](#) and the smooth evolution of bed  
 615 cover over the course of the flood imply that cover development cannot keep up with the variation in  
 616 the forcing characteristics. This dynamic adjustment of cover, which can lag forcing processes, may  
 617 thus play an important role in the dynamics of bedrock channels and probably needs to be taken into  
 618 account in modelling.



619 Fig. 12: Calculated evolution of cover during the largest event observed at the Erlenbach on 20<sup>th</sup> June  
 620 2007 (Turowski et al., 2009). Bedload transport rates were measured with the Swiss Plate geophone  
 621 sensors calibrated with direct bedload samples (Rickenmann et al., 2012). The final fraction of  
 622 exposed bedrock is strongly dependent on its initial value.  
 623

#### 624 4. Discussion

##### 625 4.1 Model formulation

627 In principle, the framework for the cover effect presented here allows the formulation of a general  
 628 model for bedrock channel morphodynamics without the restrictions of previous models (e.g. [Nelson  
 629 and Seminara, 2011](#); Zhang et al., 2015). To achieve this, the dependency of  $P$  on various control  
 630 parameters needs to be specified. In general,  $P$  should be controlled by local topography, grain size  
 631 and shape, hydraulic forcing, and the amount of sediment already residing on the bed. Furthermore,  
 632 the shape of the  $P$  function should also be affected by feedbacks between these properties, such as  
 633 the development of sediment cover altering the local roughness and hence altering hydraulics and  
 634 local transport capacity (Inoue et al., 2014; Johnson, 2014). Within the treatment presented here, we  
 635 have explicitly accounted only for the impact of the amount of sediment already [residing](#) on the bed.  
 636 However, all of the mentioned effects can be included implicitly by an appropriate choice of  $P$ . The  
 637 exact relationships between, say, bed topography and  $P$  need to be mapped out experimentally (e.g.,  
 638 Inoue et al., 2014), with theoretical approaches also providing some direction (cf. Johnson, 2014;  
 639 Zhang et al., 2015). Currently available experimental results (Chatanantavet and Parker, 2008;  
 640 Finnegan et al., 2007; Hodge and Hoey, 2016; Inoue et al., 2014; Johnson and Whipple, 2007) cover  
 641 only a small range of the possible parameter space and, [in general, do not generally report all  
 642 necessary parameters to constrain  \$P\$  were reported](#). Specifically the stationary mass of sediment  
 643 residing on the bed is [generally usually](#) not reported and can be difficult to determine

644 experimentally, but is necessary to determine  $P$ . Nevertheless, depending on the choice of  $P$ , our  
645 model can yield a wide range of cover functions that encompasses reported functions both from  
646 numerical modelling (e.g., Aubert et al., 2016; Hodge and Hoey, 2012; Johnson, 2014) and  
647 experiments (Chatanantavet and Parker, 2008; Inoue et al., 2014; Sklar and Dietrich, 2001) ([see Figs.  
648 4 and 5](#)).

649  
650 The dynamic model put forward here is a minimum first order formulation, and there are some  
651 obvious future alterations. We only take account of the static cover effect caused by immobile  
652 sediment on the bed. The dynamic cover effect, which arises when moving grains interact at high  
653 sediment concentration and thus reduce the number of impacts on the bed (Turowski et al., 2007),  
654 could in principle be included into the formulation, [but would necessitate a second probability  
655 function specifically to describe this dynamic cover. It would also be possible to use different  \$P\$ -  
656 functions for entrainment and deposition, thus introducing hysteresis into cover development.](#) Such  
657 hysteresis has been observed in experiments in which the equilibrium sediment cover was a function  
658 of the initial extent of sediment cover (Chatanantavet and Parker, 2008; Hodge and Hoey, 2012).  
659 Whether such alterations are necessary is best established with targeted laboratory experiments.

660

#### 661 **4.2 Comparison to previous modelling frameworks**

662 We will briefly outline in this section the main differences to previous formulations of cover dynamics  
663 in bedrock channels. Thus, the novel aspects of our formulation and the respective advantages and  
664 disadvantages will become clear.

665

666 Aubert et al. (2015) coupled the movement of spherical particles to the simulation of a turbulent  
667 fluid and investigated how cover depended on transport capacity and supply. Similar to what is  
668 predicted by our analytical formulation, they found a range of cover function for various model set-  
669 ups, including linear and convex-up relationships (compare the results in Fig. 4 to their Fig. 15).  
670 Despite short-comings, Aubert et al. (2015) presented the so far most detailed physical simulations of  
671 bed cover formation and the correspondence between the predictions is encouraging.

672

673 Nelson and Seminara (2011, 2011) formulated a morphodynamic model for bedrock channels. They  
674 based their formulation on sediment concentration, which is in principle similar to our formulation  
675 based on mass. However, Nelson and Seminara (2011, 2012) did not distinguish between mobile and  
676 stationary sediment and linked local transport directly to sediment concentration. Further, a given  
677 mass can be distributed in multiple ways to achieve various degrees of cover, a fact that is quantified  
678 in our formulation by the probability parameter  $P$ . Nelson and Seminara (2011, 2012) assumed a  
679 direct correspondence between sediment concentration and degree of cover, which is equivalent to  
680 the linear cover assumption (eq. 7), with the associated problems outlined earlier. Practically, this  
681 implies that the grid size needs to be of the order of the grain size. Although different in various  
682 details, Inoue et al. (2016) have used essentially the same approach as Nelson and Seminar (2011,  
683 2012) to link bedload concentration, transport and bed cover. Both of these models allow the 2D  
684 modelling of bedrock channel morphology. Although we have not fully developed such a model in  
685 the present paper, our model framework could easily be extended to 2D problems.

686

687 [Inoue et al. \(2014\) formulated a 1D model for cover dynamics and bedrock erosion. There, they  
688 distinguish between stationary and mobile sediment using an Exner equation to capture sediment  
689 mass conservation. The degree of bed cover is related to transport rates and sediment mass via a  
690 saturation volume, which is related to our characteristic mass  \$M\_0^\*\$  \(see section 3.2\). A key difference  
691 between Inoue et al.'s \(2014\) model and the one presented here lies in the sediment continuity](#)

692 equation (eq. 26), in which we explicitly take explicitly account of both entrainment and deposition.  
693 In addition, with the function  $P$ , describing the relationship between deposited mass and degree of  
694 cover, we provide a more flexible framework for complex simulations where the bed needs to be  
695 discretized (e.g., 2D models or reach-scale formulations).

696

697 Zhang et al. (2015) formulated a bed cover model specifically for beds with macro-roughness. There,  
698 deposited sediment always fills topographic lows from their deepest positions, such that there is a  
699 reach-uniform sediment level. While the model is interesting and provides a fundamentally different  
700 approach to what is suggested here, its applicability is limited to very rough beds and the assumption  
701 of a sediment elevation that is independent of the position on the bed seems physically unrealistic. In  
702 principle, the probabilistic framework presented here should be able to deal with macro-rough beds  
703 as well and thus allows a more general treatment of the problem of bed cover.

704

705 Within this paper, we focused on the dynamics of bed cover, rather than modelling the dynamics of  
706 entire channels. The probabilistic formulation using the parameter  $P$  provides a flexible framework  
707 to connect the sediment mass residing on the bed with the exposed bedrock fraction. This particular  
708 element has not been treated in any of the previous models and could be easily implemented in  
709 other approaches dealing with sediment fluxes along and across the stream and the interaction with  
710 erosion and, over long time scales, channel morphology. However, it is as yet unclear how flow  
711 hydraulics, sediment properties and other conditions affect  $P$  and this should be investigated in  
712 targeted laboratory experiments. Nevertheless, the proposed formulation provides a framework in  
713 which data from various sources can be easily compared and discussed.

714

#### 715 **4.3 Further implications**

716 Based on field data interpretation, Phillips and Jerolmack (2016) argued that bedrock rivers adjust  
717 such that, similar to alluvial channels, medium sized floods are most effective in transporting  
718 sediment, and that channel geometry therefore can quickly adjust their transport capacity to the  
719 applied load and therefore achieve grade (cf. Mackin, 1948). They conclude that bedrock channels  
720 can adjust their morphologic parameters (channel width and shape) quickly in response to changing  
721 boundary conditions, a somewhat counter-intuitive notion for slowly-eroding channels. Contrary to  
722 the suggestion of Phillips and Jerolmack (2016) that this is achieved by changing channel morphologic  
723 parameters such as width. In contrast, our model suggests that bed cover is can be adjusted to  
724 achieve grade. Furthermore changes in sediment cover can occur far more rapidly than  
725 morphological changes. In steady state, time derivatives need to be equal to zero. Thus, entrainment  
726 equals deposition (eq. 16), implying that the downstream gradient in sediment transport rate is equal  
727 to zero (eq. 14). When sediment supply or transport capacity change, the exposed bedrock fraction  
728 can adjust to achieve a new steady state and a change of the channel geometry is unnecessary.  
729 These changes in sediment cover can occur far more rapidly than changes in width and cross-  
730 sectional shape (compare to eq. 47). Whether a steady state is achieved depends on the relative  
731 magnitude of the timescales of perturbation and cover adjustment (see section 3.2). Our results  
732 imply that bedrock channels have two distinct time scales to adjust to changing boundary conditions  
733 to achieve grade. Over short times, bed cover is adjusted. This can occur rapidly. Over long time  
734 scales, channel width, cross-sectional shape and slope are adjusted.

735

#### 736 **5. Conclusions**

737

738 The probabilistic view put forward in this paper offers a framework into which diverse data on bed  
739 cover, whether obtained from field studies, laboratory experiments or numerical modeling, can be

740 easily converted to be meaningfully compared. The conversion requires knowledge of the mass of  
741 sediment on the bed and the evolution of exposed fraction of the bed. Within the framework,  
742 individual data sets can be compared to the exponential benchmark and linear limit cases, enabling  
743 physical interpretation. Furthermore, the formulation allows the general dynamic sub-grid modelling  
744 of bed cover. Depending on the choice of  $P$ , the model yields a wide range of possible cover  
745 functions. Which of these functions are appropriate for natural rivers and how they vary with factors  
746 including topography needs to be mapped out experimentally.

747  
748 It needs to be noted here that the precise formulation of the entrainment and deposition functions  
749 also affects steady state cover relations. When calibrating  $P$  on data, it cannot always be decided  
750 whether a specific deviation from the benchmark case results from varying entrainment and  
751 deposition processes or from changes in the probability function driven for example by variations in  
752 roughness. For the prediction of the steady state cover relations and for the comparison of data sets,  
753 this should not matter, but the dynamic evolution of cover could be strongly affected.

754  
755 The system timescale for cover adjustment is inversely related to transport capacity. This time scale  
756 can be long and in many realistic situations, cover cannot instantaneously adjust to changes in the  
757 forcing conditions. Thus, dynamic cover adjustment needs to be taken into account when modelling  
758 the long-term evolution of bedrock channels.

759  
760 Our model formulation implies that bedrock channels adjust bed cover to achieve grade. Therefore,  
761 bedrock channel evolution is driven by two optimization principles. On short time scales, bed cover  
762 adjusts to match the sediment output of a reach to its input. Over long time scales, width and slope  
763 of the channel evolve to match long-term incision rate to tectonic uplift or base level lowering rates.  
764

765 **Appendix A: Perturbation analysis**

766

767 Here, we derive the effect of a small sinusoidal perturbation of the driving variables, namely  
 768 sediment supply  $q_s^*$  and transport capacity  $q_t^*$ , on cover development. The perturbation of the  
 769 driving variables can be written as

$$q_s^* = \overline{q_s^*} + \delta q_s^*$$

770 (eq. A1)

$$q_t^* = \overline{q_t^*} + \delta q_t^*$$

771 (eq. A2)

772 Here, the bar denotes the average of the quantity at steady state, while  $\delta q_s^*$  and  $\delta q_t^*$  denote the  
 773 small perturbation. The exposed area can be similarly written as

$$A^* = \overline{A^*} + \delta A^*$$

774 (eq. A3)

775 Steady state cover is directly related to the mass on the bed  $M_s^*$  by eq. (3), which we can rewrite as

$$\frac{dA^*}{dt} = -P \frac{dM_s^*}{dt}$$

776 (eq. A4)

777 Substituting eq. (A3) and a similar equation for  $M_s^*$ ,

$$M_s^* = \overline{M_s^*} + \delta M_s^*$$

778 (eq. A5)

779 we obtain

$$\frac{d\delta A^*}{dt} = -P \frac{d\delta M_s^*}{dt}$$

780 (eq. A6)

781 Here, the averaged terms drop out as they are independent of time. If  $P$  and the steady state  
 782 solution for  $A^*$  are known, a direct relationship between  $A^*$  and  $M_s^*$  can be derived. For example, for  
 783 the exponential cover model (eq. 2), substituting eqs. (A3) and (A5), we find

$$\overline{A^*} + \delta A^* = e^{-\overline{M_s^*} - \delta M_s^*} = e^{-\overline{M_s^*}} e^{-\delta M_s^*} = \overline{A^*} e^{-\delta M_s^*} \approx \overline{A^*} (1 - \delta M_s^*)$$

784 (eq. A7)

785 Here, since the  $\delta$  variables are small, we approximated the exponential term using a Taylor expansion  
 786 to first order. We obtain

$$\delta A^* = -\overline{A^*} \delta M_s^*$$

787 (eq. A8)

788 It is therefore sufficient to derive the perturbation solution for  $M_s^*$ , the time evolution of which is  
 789 given by eq. (22). Eliminating  $M_m^*$  using eq. (24), we obtain

$$\frac{\partial M_s^*}{\partial t^*} = \left(1 - e^{-q_s^*/U^*}\right) q_s^* - \left(1 - e^{-M_s^*}\right) q_t^*$$

790 (eq. A9)

791

792 **Perturbation of sediment supply**

793

794 First, let's look at a perturbation of sediment supply  $q_s^*$ , while other parameters are held constant.  
 795 Substituting eq. (A1) and (A5) into (A9), we obtain

$$\frac{\partial \delta M_s^*}{\partial t^*} = \left(1 - e^{-\frac{(\overline{q_s^*} + \delta q_s^*)}{U^*}}\right) (\overline{q_s^*} + \delta q_s^*) - \left(1 - e^{-\overline{M_s^*} - \delta M_s^*}\right) q_t^*$$

796 (eq. A10)

797 Again, since the  $\delta$  variables are small, we can replace the relevant exponentials with Taylor expansion  
 798 to first order:

$$e^{-\delta q_s^*/U^*} \approx 1 - \frac{\delta q_s^*}{U^*}$$

799 (eq. A11)

800 A similar approximation applies for the exponential in  $M_s^*$ . Substituting eq. (A11) into eq. (A10),  
 801 expanding the multiplicative terms, dropping terms of second order in the  $\delta$  variables and  
 802 rearranging, we get

$$\frac{\partial \delta M_s^*}{\partial t^*} = \delta q_s^* \left( 1 - e^{-\frac{\bar{q}_s^*}{U^*}} + \frac{\bar{q}_s^*}{U^*} e^{-\frac{\bar{q}_s^*}{U^*}} \right) - \delta M_s^* \left( q_t^* - \left( 1 - e^{-\frac{\bar{q}_s^*}{U^*}} \right) \bar{q}_s^* \right)$$

803 (eq. A12)

804 The perturbation is assumed to be sinusoidal

$$\delta q_s^* = d \sin\left(\frac{2\pi t}{p}\right)$$

805 (eq. A13)

806 Here,  $p$  is the period of the perturbation and  $d$  is its amplitude. Note that, to be consistent with the  
 807 assumptions previously made,  $d$  needs to be small in comparison with the average sediment supply.  
 808 Substituting, eq. (A12) can be integrated to obtain the solution

$$\delta M_s^* = G_{q_s^*} \sin\left(\frac{2\pi t}{p} + \varphi_{q_s^*}\right) + C \exp\left\{-\left(q_t^* - \left(1 - e^{-\frac{\bar{q}_s^*}{U^*}}\right) \bar{q}_s^*\right) \frac{t}{T}\right\}$$

809 where  $C$  is a constant of integration. The gain is given by

$$G_{q_s^*} = \frac{p}{T} \frac{\left(1 - e^{-\frac{\bar{q}_s^*}{U^*}} + \frac{\bar{q}_s^*}{U^*} e^{-\frac{\bar{q}_s^*}{U^*}}\right) d}{\sqrt{\left(q_t^* - \left(1 - e^{-\frac{\bar{q}_s^*}{U^*}}\right) \bar{q}_s^*\right)^2 \left(\frac{p}{T}\right)^2 + 4\pi^2}}$$

810 (eq. A14)

811 And the phase shift by

$$\varphi_{q_s^*} = \tan^{-1} \left[ \frac{2\pi}{\frac{p}{T} \left(q_t^* - \left(1 - e^{-\frac{\bar{q}_s^*}{U^*}}\right) \bar{q}_s^*\right)} \right]$$

812 (eq. A15)

813

814 **Perturbation of transport capacity**



815  
816  
817  
818  
819  
820

The perturbation of the transport capacity  $q_t^*$  is a little more complicated, since both  $q_t^*$  and  $U^*$  are explicitly dependent on hydraulics (e.g., shear stress; see eqs. 43 and 44), and thus  $U^*$  is implicitly dependent on  $q_t^*$  and  $\delta q_t^*$ . To circumvent this problem, we expand the exponential term featuring  $U^*(\delta q_t^*)$  in eq. (A9) using a Taylor series expansion around  $\delta q_t^* = 0$ .

$$\exp\left\{-\frac{q_s^*}{U^*(\delta q_t^*)}\right\} \approx \exp\left\{-\frac{q_s^*}{U^*(\delta q_t^* = 0)}\right\} \left[1 - \frac{q_s^*}{U^{*2}(\delta q_t^* = 0)} \frac{\partial U^*}{\partial \delta q_t^*}(\delta q_t^* = 0) \delta q_t^*\right]$$

821 (eq. A16)

822 Both  $U^*$  and its derivative are constants when evaluated at  $\delta q_t^* = 0$ . We can thus write

823

$$\exp\left\{-\frac{q_s^*}{U^*}\right\} = \exp\left\{-\frac{q_s^*}{U^*}\right\} \left[1 - \frac{q_s^*}{U^{*2}} \left(\frac{\partial U^*}{\partial \delta q_t^*}\right) \delta q_t^*\right] = [1 - C_0 \delta q_t^*] e^{-q_s^*/U^*}$$

824

825 (eq. A17)

826 Here,  $C_0$  is a constant. Proceeding as before by substituting eq. (A2), (A8) and (A17) into (A9),

827 expanding exponential terms containing  $\delta$  variables, dropping terms of second order in the  $\delta$

828 variables and rearranging, we obtain:

$$\frac{\partial \delta M_s^*}{\partial t^*} = \left( B q_s^* e^{-q_s^*/U^*} + e^{-\overline{M}_s^*} - 1 \right) \delta q_t^* - \delta M_s^* \overline{q_t^*} e^{-\overline{M}_s^*}$$

829 (eq. A18)

830 A sinusoidal perturbation of the form

$$\delta q_t^* = d \sin\left(\frac{2\pi t}{p}\right)$$

831 (eq. A19)

832 yields the solution

$$\delta M_s^* = G_{q_t^*} \sin\left(\frac{2\pi t}{p} + \varphi_{q_t^*}\right) + C \exp\left\{-\left(\overline{q_t^*} - \left(1 - e^{-q_s^*/U^*}\right) q_s^*\right) \frac{t}{p}\right\} \left\{-\left(\overline{q_t^*} - \left(1 - e^{-q_s^*/U^*}\right) q_s^*\right) \frac{t}{T}\right\}$$

833 with

$$G_{q_t^*} = \frac{p}{T} \frac{\left(\frac{q_s^{*2}}{U^{*2}} \left(\frac{\partial U^*}{\partial \delta q_t^*}\right) e^{-q_s^*/U^*} - \left(1 - e^{-q_s^*/U^*}\right) \frac{q_s^*}{q_t^*}\right) d}{\sqrt{\overline{q_t^*}^2 \left(\frac{p}{T}\right)^2 \left(1 - \left(1 - e^{-q_s^*/U^*}\right) \frac{q_s^*}{q_t^*}\right)^2 + 4\pi^2}}$$

834 (eq. A20)

835 and

$$\varphi = \tan^{-1}\left(-\frac{2\pi}{\frac{p}{T} \left(\overline{q_t^*} - \left(1 - e^{-q_s^*/U^*}\right) q_s^*\right)}\right)$$

836 (eq. A21)

837

### 838 Summary

839

840 Using the system timescale  $T_s$ , the phase shift and gain can be generally rewritten as

841

$$\varphi = \tan^{-1}\left(-2\pi \frac{T_s}{p}\right)$$

842 (eq. A22)

$$G = \frac{p}{T_s} \frac{Kd}{\sqrt{\left(\frac{p}{T_s}\right)^2 + 4\pi^2}}$$

843 (eq. A23)

844 Here,  $K$  differs for perturbations in sediment supply and transport capacity, given by the equations

845

$$K_{q_s^*} = 1 - e^{-\frac{\bar{q}_s^*}{U^*}} + \frac{\bar{q}_s^*}{U^*} e^{-\frac{\bar{q}_s^*}{U^*}}$$

846 (eq. A24)

$$K_{q_t^*} = \frac{q_s^{*2}}{U^{*2}} \overline{\left(\frac{\partial U^*}{\partial \delta q_t^*}\right)} e^{-q_s^*/U^*} - \left(1 - e^{-q_s^*/U^*}\right) \frac{q_s^*}{q_t^*}$$

847 (eq. A25)

848

849

850 **Notation**

851

852 Overbars denote time-averaged quantities.

853

854  $a$  Shape parameter in the regularized incomplete Beta function.

855  $A^*$  Fraction of exposed (uncovered) bed area.

856  $A_c^*$  Fraction of covered bed area.

857  $b$  Shape parameter in the regularized incomplete Beta function.

858  $B$  Regularized incomplete Beta function.

859  $C$  Constant of integration.

860  $C_0$  Constant [ $\text{m}^2\text{s}/\text{kg}$ ].

861  $d$  Amplitude of perturbation [ $\text{kg}/\text{m}^2\text{s}$ ].

862  $D$  Sediment deposition rate per bed area [ $\text{kg}/\text{m}^2\text{s}$ ].

863  $D^*$  Dimensionless sediment deposition rate.

864  $D_{50}$  Median grain size [m].

865  $e$  Base of the natural logarithm.

866  $E$  Sediment entrainment rate per bed area [ $\text{kg}/\text{m}^2\text{s}$ ].

867  $E^*$  Dimensionless sediment entrainment rate.

868  $E_{max}$  Maximal possible dimensionless sediment entrainment rate.

869  $g$  Acceleration due to gravity [ $\text{m}/\text{s}^2$ ].

870  $G$  Gain [ $\text{kg}/\text{m}^2\text{s}$ ].

871  $I$  Non-dimensional incision rate.

872  $k$  Probability of sediment deposition on uncovered parts of the bed, linear  
873 implementation.

874  $k_I$  Non-dimensional erodibility.

875  $K$  Parameter in the gain equation.

876  $L$  Characteristic length scale [m].

877  $M_0$  Minimum mass per area necessary to cover the bed [ $\text{kg}/\text{m}^2$ ].

878  $M_0^*$  Dimensionless characteristic sediment mass.

879  $M_m$  Mobile sediment mass [ $\text{kg}/\text{m}^2$ ].

880  $M_m^*$  Dimensionless mobile sediment mass.

881  $M_s$  Stationary sediment mass [ $\text{kg}/\text{m}^2$ ].

882  $M_s^*$  Dimensionless stationary sediment mass.

883  $p$  Period of perturbation [s].

884  $p_c$  Probability of entrainment, CA model, blocked grains.

885  $p_f$  Probability of entrainment, CA model, free grains.

886

887  $P$  Probability of sediment deposition on uncovered parts of the bed.

888  $q_s$  Mass sediment transport rate per unit width [ $\text{kg}/\text{ms}$ ].

889  $q_s^*$  Dimensionless sediment transport rate.

890  $q_t$  Mass sediment transport capacity per unit width [ $\text{kg}/\text{ms}$ ].

891  $q_t^*$  Dimensionless transport capacity.

892  $Q_s^*$  Relative sediment supply; sediment transport rate over transport capacity.

893  $Q_t$  Mass sediment transport capacity [ $\text{kg}/\text{s}$ ].

894  $t$  Time variable [s].

895  $t^*$  Dimensionless time.

896  $T$  Characteristic time scale [s].

897  $T_E$  Characteristic time scale for sediment entrainment [s].

898	$T_S$	Characteristic system time scale [s].
899	$U$	Sediment speed [m/s].
900	$U^*$	Dimensionless sediment speed.
901	$x$	Dimensional streamwise spatial coordinate [m].
902	$x^*$	Dimensionless streamwise spatial coordinate.
903	$y$	Dummy variable.
904	$\alpha$	Exponent.
905	$\gamma$	Fraction of pore space in the sediment.
906	$\delta$	denotes time-varying component.
907	$\theta$	Shields stress.
908	$\theta_c$	Critical Shields stress.
909	$\rho$	Density of water [kg/m <sup>3</sup> ].
910	$\rho_s$	Density of sediment [kg/m <sup>3</sup> ].
911	$\tau$	Bed shear stress [N/m <sup>2</sup> ].
912	$\tau_c$	Critical bed shear stress at the onset of bedload motion [N/m <sup>2</sup> ].
913		
914		

915 **Acknowledgements**

916

917 We thank Joel Scheingross and Jean Braun for insightful discussions [and two anonymous reviewers](#)  
918 [fro insightful comments on a previous version of the manuscript](#). The data from the Erlenbach is  
919 owned by and is used with permission of the Mountain Hydrology and Mass Movements Group at  
920 the Swiss Federal Research Institute for Forest Snow and Landscape Research WSL.

921

922 **References**

923

- 924 Aubert, G., Langlois, V.J., Allemand, P. (2016). Bedrock incision by bedload: Insights from direct  
925 numerical simulations. *Earth Surf. Dynam.*, 4, 327-342, doi: 10.5194/esurf-4-327-2016
- 926 Beer, A. R., & Turowski, J. M. (2015). Bedload transport controls bedrock erosion under sediment-  
927 starved conditions. *Earth Surface Dynamics*, 3, 291-309, doi: 10.5194/esurf-3-291-2015
- 928 Beer, A. R., Turowski, J. M., Fritschi, B., Rieke-Zapp, D. H. (2015). Field instrumentation for high-  
929 resolution parallel monitoring of bedrock erosion and bedload transport, *Earth Surface*  
930 *Processes and Landforms*, 40, 530-541, doi: 10.1002/esp.3652
- 931 Beer, A. R., Kirchner, J. W., Turowski, J. M. (2016). Graffiti for science – erosion painting reveals  
932 spatially variable erosivity of sediment-laden flows, *Earth Surface Dynamics*, 4, 885-894, doi:  
933 10.5194/esurf-4-885-2016
- 934 Charru, F., Mouilleron, H., Eiff, O. (2004). Erosion and deposition of particles on a bed sheared by a  
935 viscous flow. *J. Fluid Mech.*, 519, 55-80
- 936 Chatanantavet, P. & Parker, G. (2008). Experimental study of bedrock channel alluviation under  
937 varied sediment supply and hydraulic conditions. *Water Resour. Res.*, 44, W12446, doi:  
938 10.1029/2007WR006581
- 939 Cook, K.; Turowski, J. M. & Hovius, N. (2013). A demonstration of the importance of bedload  
940 transport for fluvial bedrock erosion and knickpoint propagation. *Earth Surf. Process.*  
941 *Landforms*, 38, 683-695, doi: 10.1002/esp.3313
- 942 Fernandez Luque, R. & van Beek, R. (1976). Erosion and transport of bed-load sediment. *J. Hydraul.*  
943 *Res.*, 14, 127-144
- 944 Finnegan, N. J.; Sklar, L. S. & Fuller, T. K. (2007). Interplay of sediment supply, river incision, and  
945 channel morphology revealed by the transient evolution of an experimental bedrock channel.  
946 *Journal of Geophysical Research*, 112, F03S11, doi: 10.1029/2006JF000569
- 947 Gilbert, G. K. (1877), Report on the geology of the Henry Mountains: Geographical and geological  
948 survey of the Rocky Mountain region, U.S. Gov. Print. Off., Washington, D. C.
- 949 Hobbey, D. E. J.; Sinclair, H. D.; Mudd, S. M. & Cowie, P. A. (2011). Field calibration of sediment flux  
950 dependent river incision. *J. Geophys. Res.*, 116, F04017, doi: 10.1029/2010JF001935
- 951 Hodge, R.A. (in press) Sediment processes in bedrock-alluvial rivers: Research since 2010 and  
952 modelling the impact of fluctuating sediment supply on sediment cover. In: Tsutsumi, D. &  
953 Laronne, J. *Gravel-Bed Rivers: Process and Disasters*. Wiley-Blackwell.
- 954 Hodge, R. A. & Hoey, T. B. (2012). Upscaling from grain-scale processes to alluviation in bedrock  
955 channels using a cellular automaton model. *J. Geophys. Res.*, 117, F01017, doi:  
956 10.1029/2011JF002145
- 957 Hodge, R. A., T. B. Hoey, and L. S. Sklar (2011), Bedload transport in bedrock rivers: the role of  
958 sediment cover in grain entrainment, translation and deposition, *J. Geophys. Res.*, 116,  
959 F04028, doi: 10.1029/2011JF002032.
- 960 Hodge, R. A., and T. B. Hoey (2016), A Froude scale model of a bedrock-alluvial channel reach: 2.  
961 Sediment cover, *J. Geophys. Res.*, in press, doi: 10.1002/2015JF003709

962 Inoue, T., N. Izumi, Y. Shimizu, G. Parker (2014). Interaction among alluvial cover, bed roughness, and  
963 incision rate in purely bedrock and alluvial-bedrock channel. *J. Geophys. Res.*, 119, 2123-  
964 2146, doi: 10.1002/2014JF003133

965 Inoue, T., T. Iwasaki, G. Parker, Y. Shimizu, N. Izumi, C.P. Stark, J. Funaki (2016). Numerical simulation  
966 of effects of sediment supply on bedrock channel morphology. *J. Hydr. Eng.*, in press, doi:  
967 10.1061/(ASCE)HY.1943-7900.0001124

968 Johnson, J.P.L. (2014). A surface roughness model for predicting alluvial cover and bed load transport  
969 rate in bedrock channels. *J. Geophys. Res.*, 119, 2147-2173, doi: 10.1002/2013JF003000

970 Johnson, J. P. & Whipple, K. X. (2007). Feedbacks between erosion and sediment transport in  
971 experimental bedrock channels. *Earth Surf. Process. Landforms*, 32, 1048-1062, doi:  
972 10.1002/esp.1471

973 Lague, D. (2010), Reduction of long-term bedrock incision efficiency by short-term alluvial cover  
974 intermittency, *J. Geophys. Res.*, 115, F02011, doi:10.1029/2008JF001210

975 Lajeunesse, E.; Malverti, L. & Charru, F. (2010). Bed load transport in turbulent flow at the grain  
976 scale: Experiments and modeling. *Journal of Geophysical Research*, 115, F04001

977 Paola, C. & Voller, V. R. (2005). A generalized Exner equation for sediment mass balance. *J. Geophys.*  
978 *Res.*, 110, F04014

979 Phillips, C.B., D.J. Jerolmack (2016). Self-organization of river channels as a critical filter on climate  
980 signals. *Science*, 352, 694-697

981 Mackin JH. (1948). Concept of the graded river. *Geological Society of America Bulletin* 59: 463-512.  
982 doi: 10.1130/0016-7606(1948)59[463:COTGR]2.0.CO;2

983 Meyer-Peter, E., and R. Mueller (1948), Formulas for bedload transport, in 2nd meeting Int. Assoc.  
984 Hydraulic Structures Res., edited, Stockholm, Sweden.

985 Molnar P, Densmore AL, McArdell BW, Turowski JM, Burlando P. (2010). Analysis of changes in the  
986 step-pool morphology and channel profile of a steep mountain stream following a large  
987 flood. *Geomorphology* 124: 85–94. DOI. 10.1016/j.geomorph.2010.08.014

988 Nelson, P. A., and G. Seminara (2011), Modeling the evolution of bedrock channel shape with erosion  
989 from saltating bed load, *Geophys. Res. Lett.*, 38, L17406, doi: 10.1029/2011GL048628

990 Nelson, P. A., and G. Seminara (2012), A theoretical framework for the morphodynamics of bedrock  
991 channels, *Geophys. Res. Lett.*, 39, L06408, doi: 10.1029/2011GL050806.

992 Nitsche, M., D. Rickenmann, J.M. Turowski, A. Badoux, J.W. Kirchner, (2011). Evaluation of bedload  
993 transport predictions using flow resistance equations to account for macro-roughness in  
994 steep mountain streams, *Water Resources Research*, 47, W08513, doi:  
995 10.1029/2011WR010645

996 Rickenmann D, Turowski JM, Fritschi B, Klaiber A, Ludwig A. (2012). Improved sediment transport  
997 measurements in the Erlenbach stream including a moving basket system. *Earth Surface*  
998 *Processes and Landforms* 37: 1000–1011, doi: 10.1002/esp.3225

999 Sklar, L. S. & Dietrich, W. (1998). River longitudinal profiles and bedrock incision models: Stream  
1000 power and the influence of sediment supply. In: *Rivers over Rock: Fluvial Processes in*  
1001 *Bedrock Channels*, E. Tinkler, K. J. & Wohl, E. E. (Eds.), American Geophysical Union, 107, 237-  
1002 260

1003 Sklar, L.S., Dietrich, W.E., (2001). Sediment and rock strength controls on river incision into bedrock.  
1004 *Geology* 29, 1087-1090, doi: 10.1130/0091-7613(2001)029<1087:SARSCO>2.0.CO;2

1005 Sklar, L. S. & Dietrich, W. E. (2004). A mechanistic model for river incision into bedrock by saltating  
1006 bed load. *Water Resour. Res.*, 40, W06301, doi: 10.1029/2003WR002496

1007 Turowski, J. M. (2009). Stochastic modeling of the cover effect and bedrock erosion. *Water Resour.*  
1008 *Res.*, 45, W03422, doi: 10.1029/2008WR007262

1009 Turowski, J. M. & Bloem, J.-P. (2016). The influence of sediment thickness on energy delivery to the  
1010 bed by bedload impacts. *Geodynamica Acta*, 28, 199-208, doi:  
1011 10.1080/09853111.2015.1047195

1012 Turowski, J. M. & Rickenmann, D. (2009). Tools and cover effects in bedload transport observations  
1013 in the Pitzbach, Austria. *Earth Surf. Process. Landforms*, 34, 26-37, doi: 10.1002/esp.1686

1014 Turowski, J. M.; Lague, D. & Hovius, N. (2007). Cover effect in bedrock abrasion: A new derivation  
1015 and its implication for the modeling of bedrock channel morphology *J. Geophys. Res.*, 112,  
1016 F04006, doi: 10.1029/2006JF000697

1017 Turowski, J. M.; Hovius, N.; Hsieh, M.-L.; Lague, D. & Chen, M.-C. (2008). Distribution of erosion  
1018 across bedrock channels. *Earth Surf. Process. Landforms*, 33, 353-363, doi: 10.1002/esp.1559

1019 Turowski JM, Yager EM, Badoux A, Rickenmann D, Molnar P. (2009). The impact of exceptional  
1020 events on erosion, bedload transport and channel stability in a step-pool channel. *Earth*  
1021 *Surface Processes and Landforms* 34: 1661–1673, doi: 10.1002/esp.1855

1022 Turowski, J.M., A. Badoux, J. Leuzinger, R. Hegglin (2013). Large floods, alluvial overprint, and  
1023 bedrock erosion. *Earth Surface Processes and Landforms*, 38, 947-958, doi: 10.1002/esp.3341

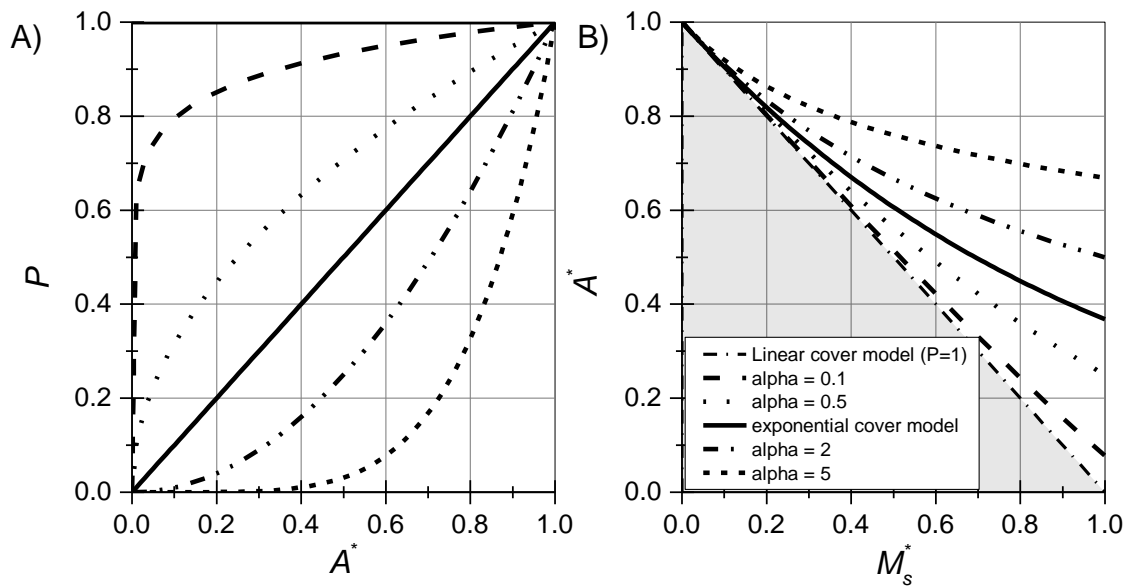
1024 Wohl, E. E. & Ikeda, H. (1997). Experimental simulation of channel incision into a cohesive substrate  
1025 at varying gradients. *Geology*, 25, 295-298, doi: 10.1130/0091-  
1026 7613(1997)025<0295:ESOCII>2.3.CO;2

1027 Wyss, C.R., D. Rickenmann, B. Fritschi, J.M. Turowski, V. Weitbrecht, R.M. Boes, (2016). Measuring  
1028 bedload transport rates by grain-size fraction using the Swiss Plate Geophone signal at the  
1029 Erlenbach, *Journal of Hydraulic Engineering*, 142(5), 04016003, doi: 10.1061/(ASCE)HY.1943-  
1030 7900.0001090

1031 Yanites, B. J.; Tucker, G. E.; Hsu, H.-L.; Chen, C.-C.; Chen, Y.-G. & Mueller, K. J. (2011). The influence of  
1032 sediment cover variability on long-term river incision rates: An example from the Peikang  
1033 River, central Taiwan. *J. Geophys. Res.*, 116, F03016, doi: 10.1029/2010JF001933

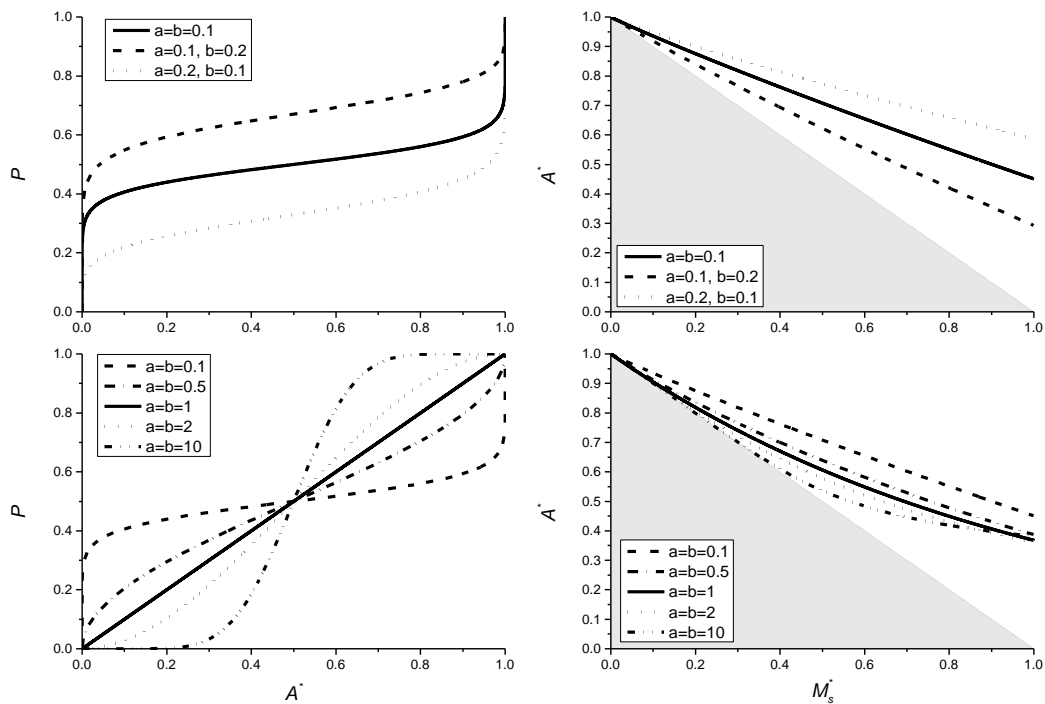
1034 Zhang, L., G. Parker, C.P. Stark, T. Inoue, E. Viparelli, X. Fu, N. Izumi (2015). Macro-roughness model  
1035 of bedrock-alluvial river morphodynamics. *Earth Surface Dynamics*, 3, 113-138, doi:  
1036 10.5194/esurf-3-113-2015

1037



1038  
1039  
1040  
1041  
1042  
1043

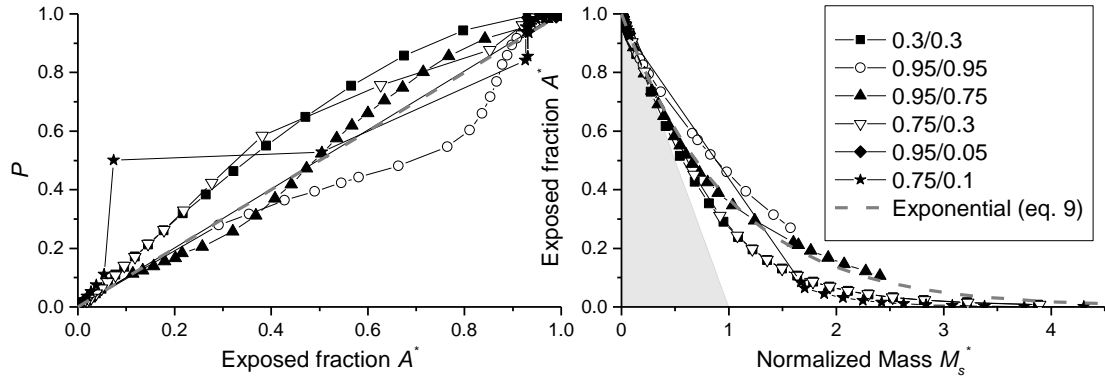
Fig. 1: A) Various examples for the probability function  $P$  as a function of bedrock exposure  $A^*$ . B) Corresponding analytical solutions for the cover function between  $A^*$  and dimensionless sediment mass  $M_s^*$  using eq. (7), (9) and (10). Grey shading depicts the area where the cover function cannot run due to conservation of mass.



1044  
1045  
1046  
1047  
1048

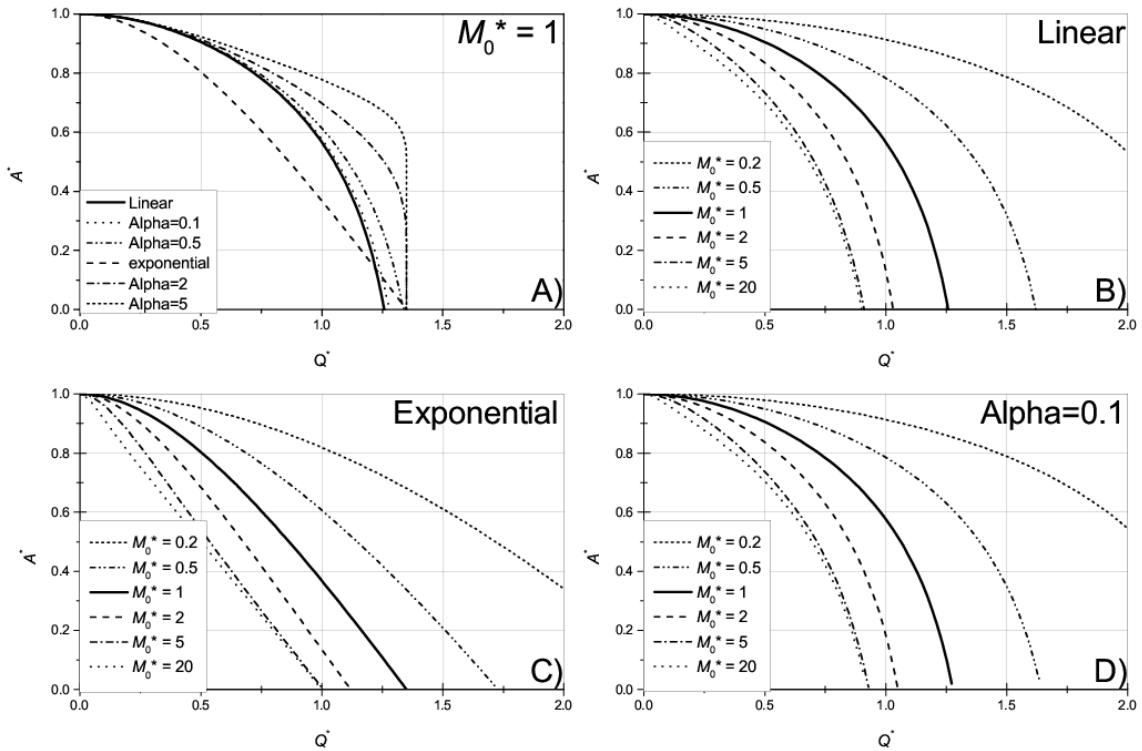
Fig. 2: Examples for the use of the regularized incomplete Beta function (eq. 12) to parameterize  $P$ , using various values for the shape parameters  $a$  and  $b$ . The choice  $a = b = 1$  gives a dependence that is equivalent to the exponential cover function. Grey shading depicts the area where the cover function cannot run due to conservation of mass.





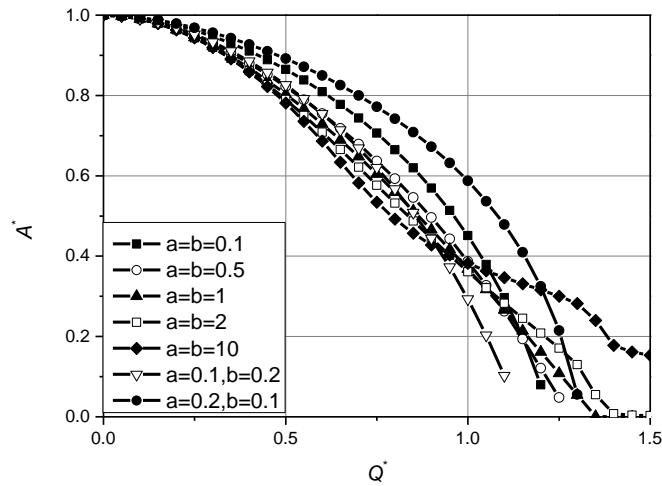
1049  
1050  
1051  
1052  
1053  
1054

Fig. 3: Probability functions  $P$  and cover function derived from data obtained from the model of Hodge and Hoey (2012). The grey dashed line shows the exponential benchmark behavior. Grey shading depicts the area where the cover function cannot run due to conservation of mass. The legend gives values of  $P_r\rho_i$  and  $P_e\rho_c$  used for the runs (see text).

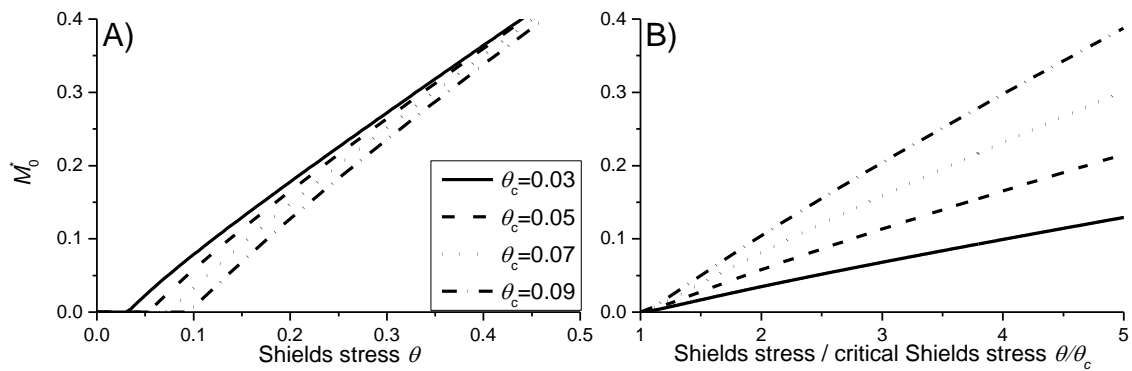


1055  
1056  
1057  
1058  
1059  
1060

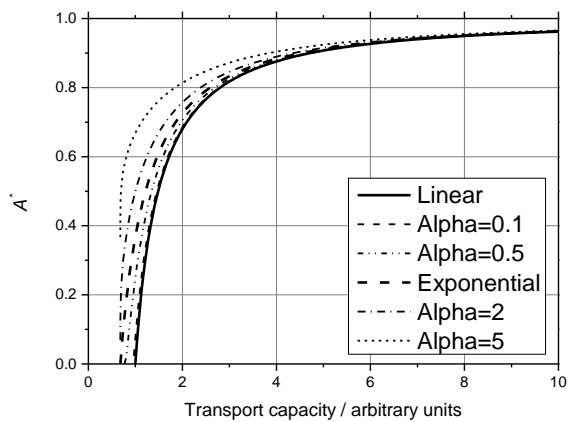
Fig. 4: Analytical solutions at steady state for the exposed fraction of the bed ( $A^*$ ) as a function of relative sediment supply ( $Q^*$ , cf. Fig. 1). A) Comparison of the different solutions, keeping  $M_0^*$  constant at 1. B) Varying  $M_0^*$  for the linear case (eq. 31). C) Varying  $M_0^*$  for the exponential case (eq. 30). D) Varying  $M_0^*$  for the power law case with  $\alpha = 0.1$  (eq. 32).



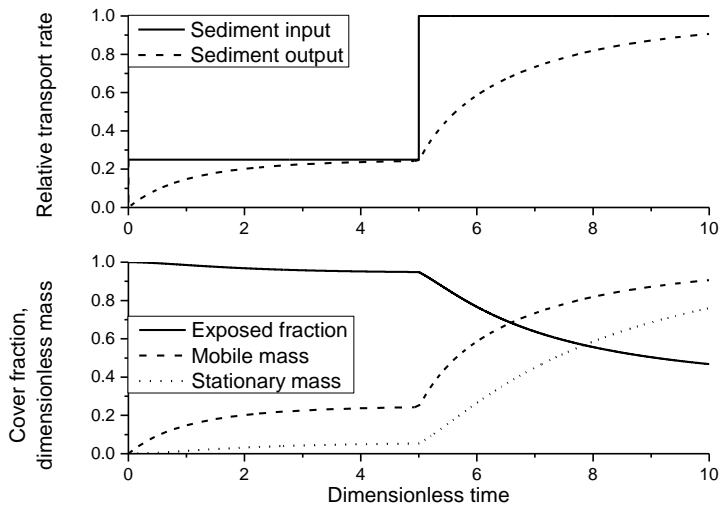
1061  
 1062 Fig. 5: Steady state solutions using the beta distribution to parameterize  $P$  (eq. 11) for a range of  
 1063 parameters  $a$  and  $b$ , and using  $M_0^* = 1$  (cf. Fig. 2). The solutions were obtained by iterating the  
 1064 equations to a steady state, using initial conditions of  $A^* = 1$  and  $M_m^* = M_s^* = 0$ .  
 1065



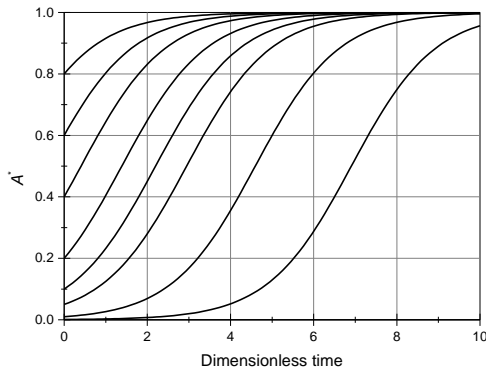
1066  
 1067 Fig. 6: The characteristic dimensionless mass  $M_0^*$  depicted as a function of A) the Shields stress and  
 1068 B) the ratio of Shields stress to critical Shields stress (eq. 37).  
 1069



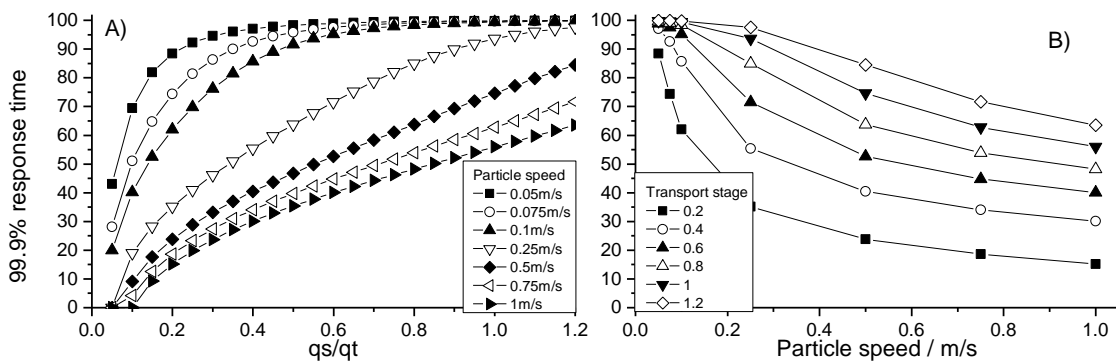
1070  
 1071 Fig. 7: Variation of the exposed bed fraction as a function of transport capacity, assuming that  
 1072 particle speed scales with transport capacity to the power of one third.  
 1073  
 1074



1075  
 1076 **Fig. 8: Temporal evolution of cover for the simple case of a control box with sediment through-flux,**  
 1077 **based on eqs. (3), (22), (23) and (24). Relative sediment supply (supply normalized by transport**  
 1078 **capacity) was specified to 0.25 and increased to 1 at  $t^* = 5$ . The response of sediment output, mobile**  
 1079 **and stationary sediment mass and the exposed bed fraction was calculated. Here, we used the**  
 1080 **exponential function for  $P$  (eq. 9) and  $M_0^* = U^* = 1$ . The initial values were  $A^* = 1$  and  $M_m^* = M_s^* =$**   
 1081 **0.** **Fig. 8: Temporal evolution of cover for a simple case. Here, we used the exponential function for  $P$**   
 1082 **(eq. 9) and  $M_0^* = 1$ . The initial values were  $A^* = 1$ ,  $M_m^* = M_s^* = 0$  and  $q_s^* = 0.25$ . Sediment supply was**  
 1083 **increased to  $q_s^* = 1$  at  $t^* = 5$ .**  
 1084

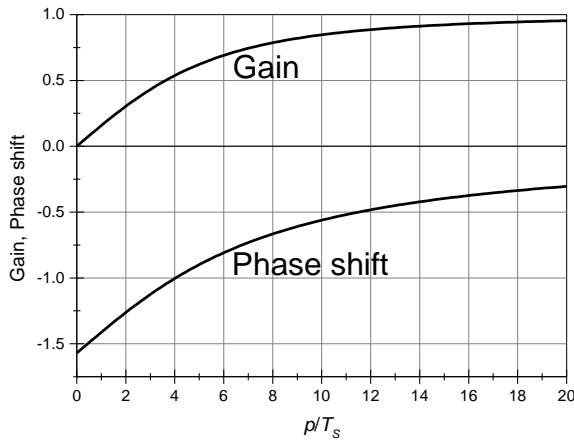


1085  
 1086 **Fig. 9: Evolution of the exposed bed fraction (removal of sediment cover) over time starting with**  
 1087 **different initial values of bed exposure, for the special case  $q_s^* = 0$  (eq. 41) and  $q_t^* = 1$ .**  
 1088

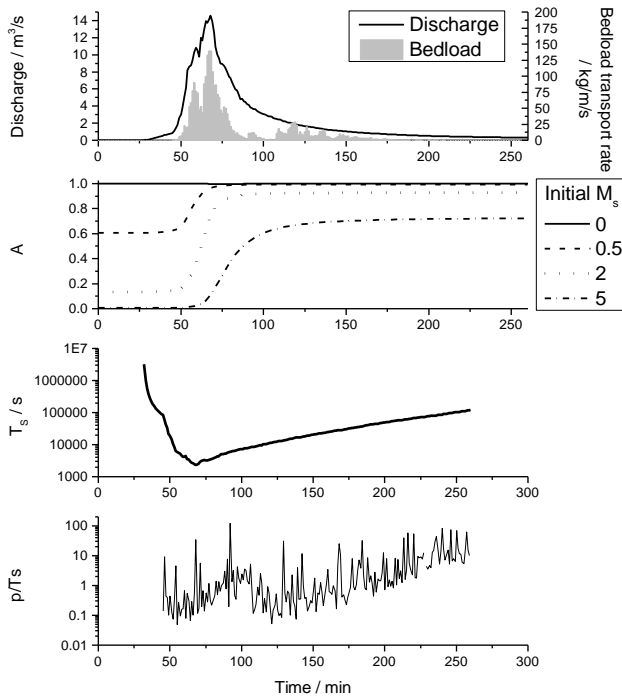


1089  
 36

1090 Fig. 10: Dimensionless time to reach 99.9% of the total adjustment in exposed area as a function of  
 1091 A) transport stage and B) particle speed. All simulation were started with  $A^* = 1$  and  $M_m^* = M_s^* = 0$ .  
 1092



1093  
 1094 Fig. 11: Phase shift (eq. 50) and gain (eq. 51) as a function of the ratio of the period of perturbation  
 1095 | period  $p$  and the system time scale  $T_s$ . For the calculation, the constant factor in the gain ( $Kd$ ) was set  
 1096 equal to one.  
 1097



1098  
 1099 Fig. 12: Calculated evolution of cover during the largest event observed at the Erlenbach on 20<sup>th</sup> June  
 1100 2007 (Turowski et al., 2009). Bedload transport rates were measured with the Swiss Plate geophone  
 1101 sensors calibrated with direct bedload samples (Rickenmann et al., 2012). The final fraction of  
 1102 exposed bedrock is strongly dependent on its initial value.  
 1103